

Meta-analysis fine-mapping is often miscalibrated at single-variant resolution

Masahiro Kanai^{1,2,3,4,5,*}, Roy Elzur^{1,2,3}, Wei Zhou^{1,2,3}, Global Biobank Meta-analysis Initiative, Mark J Daly^{1,2,3,6}, Hilary K Finucane^{1,2,3,*}

¹Analytic and Translational Genetics Unit, Massachusetts General Hospital, Boston, MA, USA, ²Program in Medical and Population Genetics, Broad Institute of MIT and Harvard, Cambridge, MA, USA, ³Stanley Center for Psychiatric Research, Broad Institute of MIT and Harvard, Cambridge, MA, USA, ⁴Department of Biomedical Informatics, Harvard Medical School, Boston, MA, USA, ⁵Department of Statistical Genetics, Osaka University Graduate School of Medicine, Suita, Japan, ⁶Institute for Molecular Medicine Finland (FIMM), University of Helsinki, Helsinki, Finland.

* Corresponding authors: Masahiro Kanai (mkanai@broadinstitute.org) and Hilary K Finucane (finucane@broadinstitute.org)

Abstract

Meta-analysis is pervasively used to combine multiple genome-wide association studies (GWAS) into a more powerful whole. To resolve causal variants, meta-analysis studies typically apply summary statistics-based fine-mapping methods as they are applied to single-cohort studies. However, it is unclear whether heterogeneous characteristics of each cohort (*e.g.*, ancestry, sample size, phenotyping, genotyping, or imputation) affect fine-mapping calibration and recall. Here, we first demonstrate that meta-analysis fine-mapping is substantially miscalibrated in simulations when different genotyping arrays or imputation panels are included. To mitigate these issues, we propose a summary statistics-based QC method, SLALOM, that identifies suspicious loci for meta-analysis fine-mapping by detecting outliers in association statistics based on ancestry-matched local LD structure. Having validated SLALOM performance in simulations and the GWAS Catalog, we applied it to 14 disease endpoints from the Global Biobank Meta-analysis Initiative and found that 67% of loci showed suspicious patterns that call into question fine-mapping accuracy. These predicted suspicious loci were significantly depleted for having likely causal variants, such as nonsynonymous variants, as a lead variant (2.7x; Fisher's exact $P = 7.3 \times 10^{-4}$). Compared to fine-mapping results in individual biobanks, we found limited evidence of fine-mapping improvement in the GBMI meta-analyses. Although a full solution requires complete synchronization across cohorts, our approach identifies likely spurious results in meta-analysis fine-mapping. We urge extreme caution when interpreting fine-mapping results from meta-analysis.

1 Introduction

2 Meta-analysis is pervasively used to combine multiple genome-wide association studies (GWAS)
3 from different cohorts¹. Previous GWAS meta-analyses have identified thousands of loci
4 associated with complex diseases and traits, such as type 2 diabetes^{2,3}, schizophrenia^{4,5},
5 rheumatoid arthritis^{6,7}, body mass index⁸, and lipid levels⁹. These meta-analyses are typically
6 conducted in large-scale consortia (e.g., the Psychiatric Genomics Consortium [PGC], the Global
7 Lipids Genetics Consortium [GLGC], and the Genetic Investigation of Anthropometric Traits
8 [GIANT] consortium) to increase sample size while harmonizing analysis plans across
9 participating cohorts in every possible aspect (e.g., phenotype definition, quality-control [QC]
10 criteria, statistical model, and analytical software) by sharing summary statistics as opposed to
11 individual-level data, thereby avoiding data protection issues and variable legal frameworks
12 governing individual genome and medical data around the world. The Global Biobank Meta-
13 analysis Initiative (GBMI)¹⁰ is one such large-scale, international effort, which aims to establish a
14 collaborative network spanning 23 biobanks from four continents (total $n = 2.2$ million) for
15 coordinated GWAS meta-analyses, while addressing the many benefits and challenges in meta-
16 analysis and subsequent downstream analyses.

17
18 One such challenging downstream analysis is statistical fine-mapping^{11–13}. Despite the great
19 success of past GWAS meta-analyses in locus discovery, individual causal variants in associated
20 loci are largely unresolved. Identifying causal variants from GWAS associations (i.e., fine-
21 mapping) is challenging due to extensive linkage disequilibrium (LD, the correlation among
22 genetic variants), the presence of multiple causal variants, and limited sample sizes, but is rapidly
23 becoming achievable with high confidence in individual cohorts^{14–17} owing to the recent
24 development of large-scale biobanks^{18–20} and scalable fine-mapping methods^{21–23} that enable
25 well-powered, accurate fine-mapping using in-sample LD from large-scale individual-level data.
26

27 After conducting GWAS meta-analysis, previous studies^{2,7,9,24–30} have applied existing summary
28 statistics-based fine-mapping methods (e.g., approximate Bayes factor [ABF]^{31,32}, CAVIAR³³,
29 PAINTOR^{34,35}, FINEMAP^{21,22}, and SuSiE²³) just as they are applied to single-cohort studies,
30 without considering or accounting for the unavoidable heterogeneity among cohorts (e.g.
31 differences in sample size, phenotyping, genotyping, or imputation). Such heterogeneity could
32 lead to false positives and miscalibration in meta-analysis fine-mapping (**Fig. 1**). For example,
33 case-control studies enriched with more severe cases or ascertained with different phenotyping
34 criteria may disproportionately contribute to genetic discovery, even when true causal effects for
35 genetic liability are exactly the same between these studies and less severe or unascertained
36 ones. Quantitative traits like biomarkers could have phenotypic heterogeneity arising from
37 different measurement protocols and errors across studies. There might be genuine biological
38 mechanisms too, such as gene–gene (GxG) and gene–environment (GxE) interactions and
39 (population-specific) dominance variation (e.g., rs671 and alcohol dependence³⁶), that introduce
40 additional heterogeneity across studies^{37,38}. In addition to phenotyping, differences in genotyping
41 and imputation could dramatically undermine fine-mapping calibration and recall at single-variant
42 resolution, because differential patterns of missingness and imputation quality across constituent
43 cohorts of different sample sizes can disproportionately diminish association statistics of
44 potentially causal variants. Finally, although more easily harmonized than phenotyping and
45 genotyping data, subtle differences in QC criteria and analytical software may further exacerbate
46 the effect of heterogeneity on fine-mapping.
47

48 An illustrative example of such issues can be observed in the *TYK2* locus (19p13.2) in the recent
49 meta-analysis from the COVID-19 Host Genetics Initiative (COVID-19 HGI; **Fig. S1**)³⁹. This locus
50 is known for protective associations against autoimmune diseases^{6,24}, while a complete *TYK2*

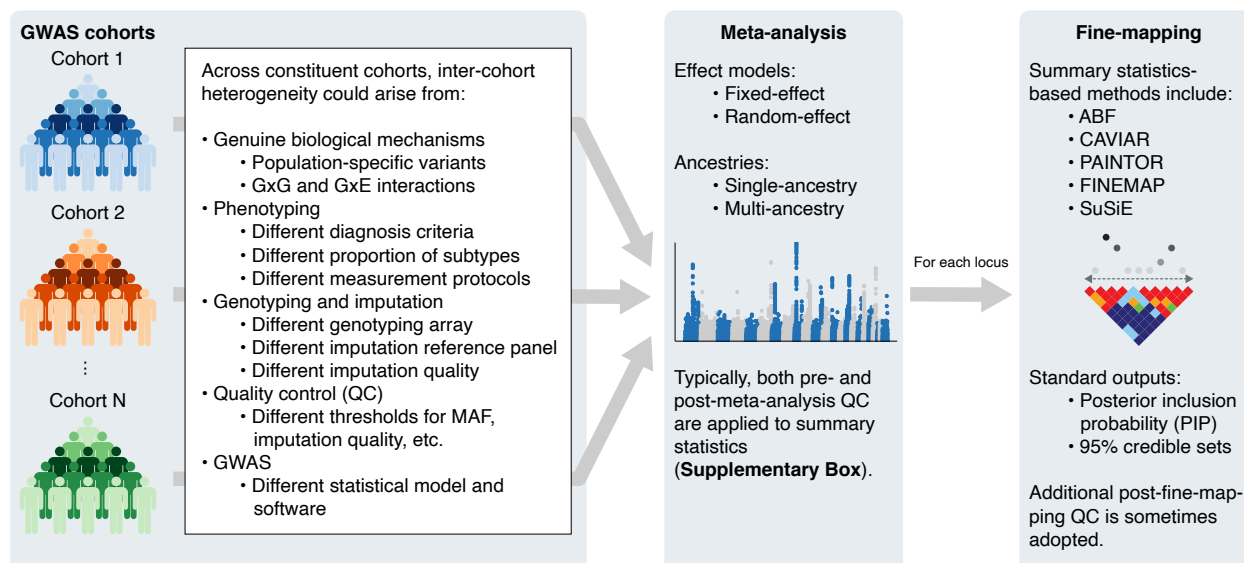
51 loss of function results in a primary immunodeficiency⁴⁰. Despite strong LD ($r^2 = 0.82$) with a lead
52 variant in the locus (rs74956615; $P = 9.7 \times 10^{-12}$), a known functional missense variant
53 rs34536443 (p.Pro1104Ala) that reduces *TYK2* function^{41,42} did not achieve genome-wide
54 significance and was assigned a very low PIP in fine-mapping ($P = 7.5 \times 10^{-7}$; PIP = 9.5×10^{-4}),
55 primarily due to its missingness in two more cohorts than rs74956615. This serves as just one
56 example of the major difficulties with meta-analysis fine-mapping at single-variant resolution.
57 Indeed, the COVID-19 HGI cautiously avoided an *in-silico* fine-mapping in the flagship to prevent
58 spurious results³⁹.

59
60 Only a few studies have carefully addressed these concerns in their downstream analyses. The
61 Schizophrenia Working Group of PGC, for example, recently updated their largest meta-analysis
62 of schizophrenia⁵ (69,369 cases and 236,642 controls), followed by a downstream fine-mapping
63 analysis using FINEMAP²¹. Unlike many other GWAS consortia, since PGC has access to
64 individual-level genotypes for a majority of samples, they were able to apply standardized sample
65 and variant QC criteria and impute variants using the same reference panel, all uniformly
66 processed using the RICOPILI pipeline⁴³. This harmonized procedure was crucial for properly
67 controlling inter-cohort heterogeneity and thus allowing more robust meta-analysis fine-mapping
68 at single-variant resolution. Furthermore, PGC's direct access to individual-level data enabled
69 them to compute in-sample LD matrices for multiple causal variant fine-mapping, which prevents
70 the significant miscalibration that results from using an external LD reference¹⁴⁻¹⁶. A 2017 fine-
71 mapping study of inflammatory bowel disease also benefited from access to individual-level
72 genotypes and careful pre- and post-fine-mapping QC⁴⁴. For a typical meta-analysis consortium,
73 however, many of these steps are infeasible as full genotype data from all cohorts is not available.
74 For such studies, a new approach to meta-analysis fine-mapping in the presence of the many
75 types of heterogeneity is needed. Until such a method is developed, QC of meta-analysis fine-
76 mapping results deserves increased attention.

77
78 While existing variant-level QC procedures are effective for limiting spurious associations in
79 GWAS (**Supplementary Box**)⁴⁵, they do not suffice for ensuring high-quality fine-mapping results.
80 In some cases, they even hurt fine-mapping quality, because they can i) cause or exacerbate
81 differential patterns of missing variants across cohorts, and ii) remove true causal variants as well
82 as suspicious variants. Thus, additional QC procedures that retain consistent variants across
83 cohorts for consideration but limit poor-quality fine-mapping results are needed. A recently
84 proposed method called DENTIST⁴⁶, for example, performs summary statistics QC to improve
85 GWAS downstream analyses, such as conditional and joint analysis (GCTA-COJO⁴⁷), by
86 removing variants based on estimated heterogeneity between summary statistics and reference
87 LD. Although DENTIST was also applied prior to fine-mapping (FINEMAP²¹), simulations only
88 demonstrated that it could improve power for detecting the correct number of causal variants in a
89 locus, not true causal variants. This motivated us to develop a new fine-mapping QC method for
90 better calibration and recall at single-variant resolution and to demonstrate its performance in
91 large-scale meta-analysis.

92
93 Here, we first demonstrate the effect of inter-cohort heterogeneity in meta-analysis fine-mapping
94 via realistic simulations with multiple heterogeneous cohorts, each with different combinations of
95 genotyping platforms, imputation reference panels, and genetic ancestries. We propose a
96 summary statistics-based QC method, SLALOM (ssuspicious loci analysis of meta-analysis
97 summary statistics), that identifies suspicious loci for meta-analysis fine-mapping by detecting
98 association statistics outliers based on local LD structure, building on the DENTIST method.
99 Applying SLALOM to 14 disease endpoints from the Global Biobank Meta-analysis Initiative¹⁰ as
100 well as 467 meta-analysis summary statistics from the GWAS Catalog⁴⁸, we demonstrate that

101 suspicious loci for fine-mapping are widespread in meta-analysis and urge extreme caution when
102 interpreting fine-mapping results from meta-analysis.
103



104
105 **Fig. 1 | Schematic overview of meta-analysis fine-mapping.**

106 Results

107 Large-scale simulations demonstrate miscalibration in meta-analysis fine-mapping

108 Existing fine-mapping methods^{21,23,31} assume that all association statistics are derived from a
109 single-cohort study, and thus do not model the per-variant heterogeneity in effect sizes and
110 sample sizes that arise when meta-analyzing multiple cohorts (**Figure 1**). To evaluate how
111 different characteristics of constituent cohorts in a meta-analysis affect fine-mapping calibration
112 and recall, we conducted a series of large-scale GWAS meta-analysis and fine-mapping
113 simulations (**Table S1–4; Methods**). Briefly, we simulated multiple GWAS cohorts of different
114 ancestries (10 European ancestry, one African ancestry and one East Asian ancestry cohorts; n
115 = 10,000 each) that were genotyped and imputed using different genotyping arrays (Illumina
116 Omni2.5, Multi-Ethnic Global Array [MEGA], and Global Screening Array [GSA]) and imputation
117 reference panels (the 1000 Genomes Project Phase 3 [1000GP3]⁴⁹, the Haplotype Reference
118 Consortium [HRC]⁵⁰, and the TOPMed⁵¹). For each combination of cohort, genotyping array, and
119 imputation panel, we conducted 300 GWAS with randomly simulated causal variants that
120 resemble the genetic architecture of a typical complex trait, including minor allele frequency (MAF)
121 dependent causal effect sizes⁵², total SNP heritability⁵³, functional consequences of causal
122 variants¹⁷, and levels of genetic correlation across cohorts (*i.e.*, true effect size heterogeneity; r_g
123 = 1, 0.9, and 0.5; see **Methods**). We then meta-analyzed the single-cohort GWAS results across
124 10 independent cohorts based on multiple *configurations* (different combinations of genotyping
125 arrays and imputation panels for each cohort) to resemble realistic meta-analysis of multiple
126 heterogeneous cohorts (**Table S4**). We applied ABF fine-mapping to compute a posterior
127 inclusion probability (PIP) for each variant and to derive 95% and 99% credible sets (CS) that
128 contain the smallest set of variants covering 95% and 99% of probability of causality. We
129 evaluated the false discovery rate (FDR, defined as the proportion of variants with PIP > 0.9 that
130 are non-causal) and compared against the expected proportion of non-causal variants if the meta-
131 analysis fine-mapping method were calibrated, based on PIP. More details of our simulation
132 pipeline are described in **Methods** and visually summarized in **Fig. S2**.

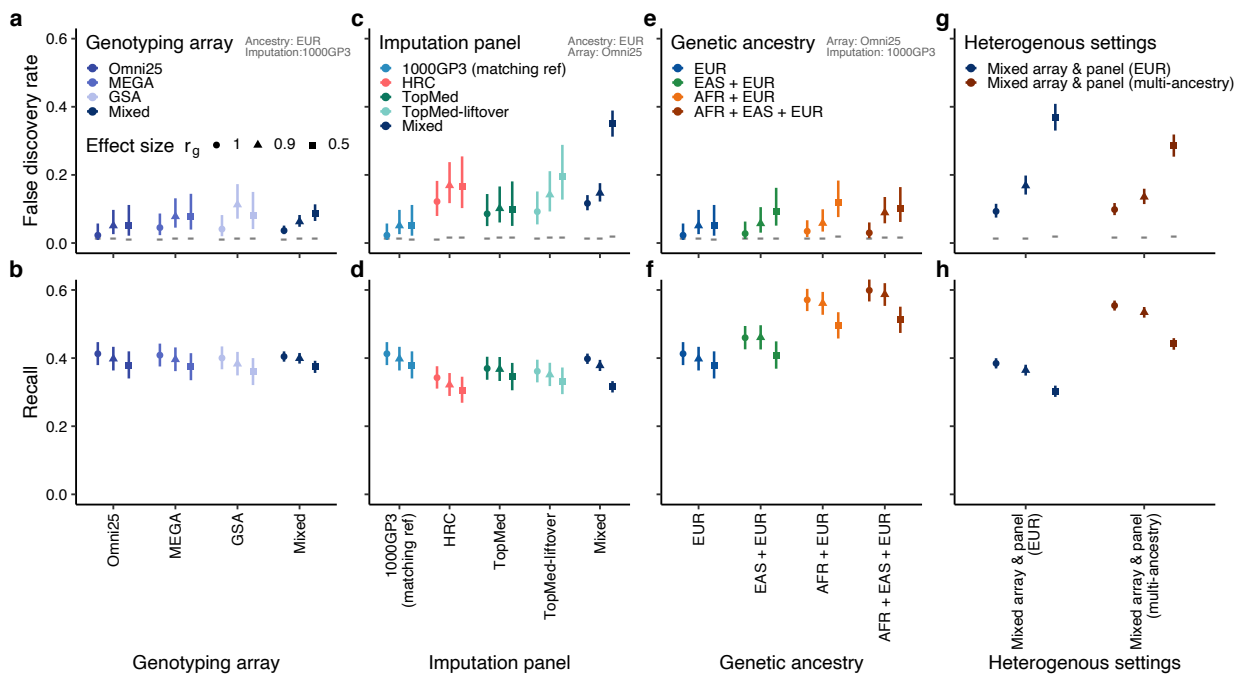
133
134 We found that FDR varied widely over the different configurations, reaching as high as 37% for
135 the most heterogeneous configurations (**Fig. 2**). We characterized the contributing factors to the
136 miscalibration. We first found that lower true effect size correlation r_g (*i.e.*, larger phenotypic
137 heterogeneity) always caused higher miscalibration and lower recall. Second, when using the
138 same imputation panel (1000GP3), use of less dense arrays (MEGA or GSA) led to moderately
139 inflated FDR (up to FDR = 11% vs. expected 1%), while use of multiple genotyping array did not
140 cause further FDR inflation (**Fig. 2a**). Third, when using the same genotyping array (Omni2.5),
141 use of imputation panels (HRC or TOPMed) that does not match our simulation reference
142 significantly affects miscalibration (up to FDR = 17% vs. expected 1%), and using multiple
143 imputation panels further increased miscalibration (up to FDR = 35% vs. expected 2%, **Fig. 2c**);
144 this setup is as bad as the most heterogeneous configuration using multiple genotyping arrays
145 and imputation panels (FDR = 37%). When TOPMed-imputed variants were lifted over from
146 GRCh38 to GRCh37, we observed FDR increases of up to 10%, likely due to genomic build
147 conversion failures (**Supplementary Note**)⁵⁴. Fourth, recall was not significantly affected by
148 heterogeneous genotyping arrays or imputation panels (**Fig. 2b,d**). Fifth, including multiple
149 genetic ancestries did not affect calibration when using the same genotyping array and imputation
150 panel (Omni 2.5 and 1000GP3; **Fig. 2e**) but significantly improved recall if African ancestry was
151 included (**Fig. 2f**). This is expected, given the shorter LD length in the African population
152 compared to other populations, which improves fine-mapping resolution⁵⁵. Finally, in the most
153 heterogeneous configurations where multiple genotyping arrays and imputation panels existed,
154 we observed a FDR of up to 37% and 28% for European and multi-ancestry meta-analyses,
155 respectively (vs. expected 2% for both), demonstrating that inter-cohort heterogeneity can
156 substantially undermine meta-analysis fine-mapping (**Fig. 2g,h**).
157

158 To further characterize observed miscalibration in meta-analysis fine-mapping, we investigated
159 the availability of GWAS variants in each combination of ancestry, genotyping array, and
160 imputation panel. Out of 3,285,617 variants on chromosome 3 that passed variant QC in at least
161 one combination (per-combination MAF > 0.001 and Rsq > 0.6; **Methods**), 574,261 variants
162 (17%) showed population-level gnomAD MAF > 0.001 in every ancestry that we simulated
163 (African, East Asian, and European). Because we used a variety of imputation panels, we
164 retrieved population-level MAF from gnomAD. Of these 574,261 variants, 389,219 variants (68%)
165 were available in every combination (**Fig. S3a**). This fraction increased from 68% to 73%, 74%,
166 and 76% as we increased gnomAD MAF thresholds to > 0.005, 0.01, and 0.05, respectively, but
167 never reached 100% (**Fig. S4**). Notably, we observed a substantial number of variants that are
168 unique to a certain genotyping array and an imputation panel, even when we restricted to 344,497
169 common variants (gnomAD MAF > 0.05) in every ancestry (**Fig. S3b**). For example, there are
170 34,317 variants (10%) that were imputed in the 1000GP3 and TOPMed reference but not in the
171 HRC. Likewise, we observed 33,106 variants (10%) that were specific to the 1000GP3 reference
172 and even 3,066 variants (1%) that were imputed in every combination except for East Asian
173 ancestry with the GSA array and the TOPMed reference. When using different combinations of
174 gnomAD MAF thresholds (> 0.001, 0.005, 0.01, or 0.05 in every ancestry) and Rsq thresholds (>
175 0.2, 0.4, 0.6, or 0.8), we observed the largest fraction of shared variants (78%) was achieved with
176 gnomAD MAF > 0.01 and Rsq > 0.2 while the largest number of the shared variants (427,494
177 variants) was achieved with gnomAD MAF > 0.001 and Rsq > 0.2, leaving it unclear which
178 thresholds would be preferable in the context of fine-mapping (**Fig. S4**).
179

180 The remaining 2,711,356 QC-passing variants in our simulations (gnomAD MAF \leq 0.001 in at
181 least one ancestry) further exacerbate variable coverage of the available variants (**Fig. S3c**). Of
182 these, the largest proportion of variants (39%) were only available in African ancestry, followed

183 by African and European (but not in East Asian) available variants (7%), European-specific
 184 variants (6%), and East Asian-specific variants (5%). Furthermore, similar to the aforementioned
 185 common variants, we found a substantial number of variants that are unique to a certain
 186 combination. Altogether, we observed that only 393,471 variants (12%) out of all the QC-passing
 187 3,285,617 variants were available in every combination (**Fig. S3d**). These observations
 188 recapitulate that different combinations of genetic ancestry, genotyping array, imputation panels,
 189 and QC thresholds substantially affect the availability of common, well-imputed variants for
 190 association testing⁵⁶.

191
 192 Thus, the different combinations of genotyping and imputation cause each cohort in a meta-
 193 analysis to have a different set of variants, and consequently variants can have very different
 194 overall sample sizes. In our simulations with the most heterogeneous configurations, we found
 195 that 66% of the false positive loci (where a non-causal [false positive] variant was assigned PIP
 196 > 0.9) had different sample sizes for true causal and false positive variants (median
 197 maximum/minimum sample size ratio = 1.4; **Fig. S5**). Analytically, we found that at common meta-
 198 analysis sample sizes and genome-wide significant effect size regimes, when two variants have
 199 similar marginal effects, the one with the larger sample size will usually achieve a higher ABF PIP
 200 (**Supplementary Note; Fig. S6–8**). This elucidates the mechanism by which sample size
 201 imbalance can lead to miscalibration.
 202
 203



204
 205 **Fig. 2 | Evaluation of false discovery rate (FDR) and recall in meta-analysis fine-mapping simulations.** We
 206 evaluated FDR and recall in meta-analysis fine-mapping using different genotyping arrays (**a,b**), imputation reference
 207 panels (**c,d**), genetic ancestries (**e, f**), and more heterogeneous settings by combining these (**g, h**). As shown in top-
 208 right gray labels, the EUR ancestry, the Omni2.5 genotyping array and/or the 1000GP3 reference panel were used
 209 unless otherwise stated. FDR is defined as the proportion of non-causal variants with PIP > 0.9. Horizontal gray lines
 210 represent 1 – mean PIP, *i.e.* expected FDR were the method calibrated. Recall is defined as the proportion of true
 211 causal variants in the top 1% PIP bin. Shapes correspond to the true effect size correlation r_g across cohorts which
 212 represent a phenotypic heterogeneity parameter (the lower r_g , the higher phenotypic heterogeneity).

213 Overview of the SLALOM method

214 To address the challenges in meta-analysis fine-mapping discussed above, we developed
215 SLALOM (ssuspicious loci analysis of meta-analysis summary statistics), a method that flags
216 suspicious loci for meta-analysis fine-mapping by detecting outliers in association statistics based
217 on deviations from expectation, estimated with local LD structure (**Methods**). SLALOM consists
218 of three steps, 1) defining loci and lead variants based on a 1 Mb window, 2) detecting outlier
219 variants in each locus using meta-analysis summary statistics and an external LD reference
220 panel, and 3) identifying suspicious loci for meta-analysis fine-mapping (**Fig. 3a,b**).

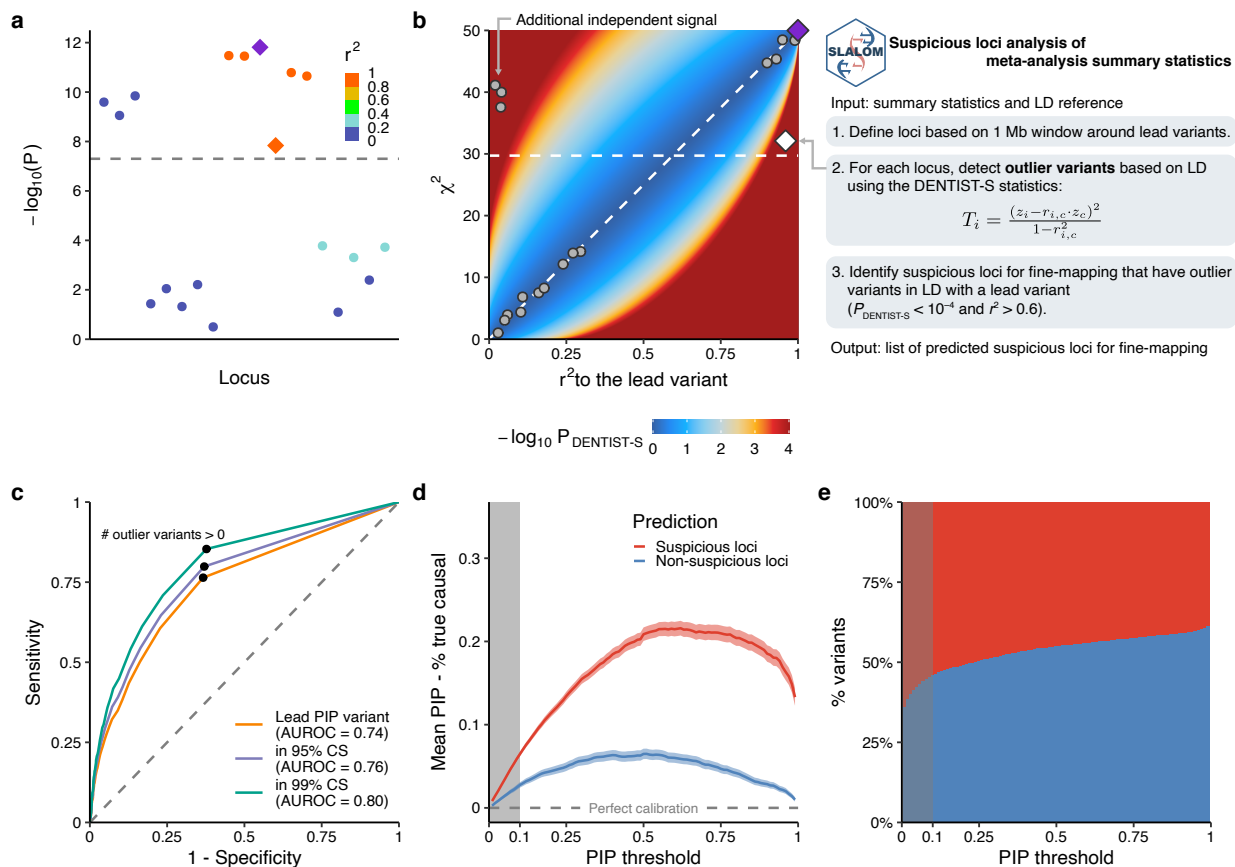
221
222 To detect outlier variants, we first assume a single causal variant per associated locus. Then the
223 marginal z-score z_i for a variant i should be approximately equal to $r_{i,c} \cdot z_c$ where z_c is the z-score
224 of the causal variant c , and $r_{i,c}$ is a correlation between variants i and c . For each variant in meta-
225 analysis summary statistics, we first test this relationship using a simplified version of the
226 DENTIST statistics⁴⁶, DENTIST-S, based on the assumption of a single causal variant. The
227 DENTIST-S statistics for a given variant i is written as

$$228 \quad T_i = \frac{(z_i - r_{i,c} z_c)^2}{1 - r_{i,c}^2} \quad (1)$$

230
231 which approximately follows a χ^2 distribution with 1 degree of freedom⁴⁶. Since the true causal
232 variant and LD structure are unknown in real data, we approximate the causal variant as the lead
233 PIP variant in the locus (the variant with the highest PIP) and use a large-scale external LD
234 reference from gnomAD⁵⁷, either an ancestry-matched LD for a single-ancestry meta-analysis or
235 a sample-size-weighted LD by ancestries for a multi-ancestry meta-analysis (**Methods**). We note
236 that the existence of multiple independent causal variants in a locus would not affect SLALOM
237 precision but would decrease recall (see **Discussion**).

238
239 SLALOM then evaluates whether each locus is “suspicious”—that is, has a pattern of meta-
240 analysis statistics and LD that appear inconsistent and therefore call into question the fine-
241 mapping accuracy. By training on loci with maximum PIP > 0.9 in the simulations, we determined
242 that the best-performing criterion for classifying loci as true or false positives is whether a locus
243 has a variant with $r^2 > 0.6$ to the lead and DENTIST-S P -value < 1.0×10^{-4} (**Methods**). Using this
244 criterion we achieved an area under the receiver operating characteristic curve (AUROC) of 0.74,
245 0.76, and 0.80 for identifying whether a true causal variant is a lead PIP variant, in 95% credible
246 set (CS), and in 99% CS, respectively (**Fig. 3c**). Using different thresholds, we observed that the
247 SLALOM performance is not very sensitive to thresholds near the threshold we chose (**Fig. S9**).
248 We further validated the performance of SLALOM using all the loci in the simulations and
249 observed significantly higher miscalibration in predicted suspicious loci than in non-suspicious
250 loci (up to 16% difference in FDR at PIP > 0.9; **Fig. 3d**). We found that SLALOM-predicted
251 “suspicious” loci tend to be from more heterogeneous configurations and the SLALOM sensitivity
252 and specificity depends on the level of heterogeneity (**Table S5**). Given the relatively lower
253 miscalibration and specificity at low PIP thresholds (**Fig. 3d,e**), in subsequent real data analysis
254 we restricted the application of SLALOM to loci with maximum PIP > 0.1 (**Methods**).

255



256
257
258 **Fig. 3 | Overview of the SLALOM method.** **a,b.** An illustrative example of the SLALOM application. **a.** In an example
259 locus, two independent association signals are depicted: i) the most significant signal that contains a lead variant (purple
260 diamond) and five additional variants that are in strong LD ($r^2 > 0.9$) with the lead variant, and ii) an additional
261 independent signal ($r^2 < 0.05$). There is one outlier variant (orange diamond) in the first signal that deviates from the
262 expected association based on LD. **b.** Step-by-step procedure of the SLALOM method. For outlier variant detection in
263 a locus, a diagnosis plot of r^2 values to the lead variant vs. marginal χ^2 is shown to aid interpretation. Background color
264 represents a theoretical distribution of $-\log_{10} P_{\text{DENTIST-S}}$ values when a lead variant has a marginal χ^2 of 50, assuming
265 no allele flipping. Points represent the variants depicted in the example locus (**a**), where the lead variant (purple
266 diamond) and the outlier variant (white diamond) were highlighted. Diagonal line represents an expected marginal
267 association. Horizontal dotted lines represent the genome-wide significance threshold ($P < 5.0 \times 10^{-8}$). **c.** The ROC
268 curve of SLALOM prediction for identifying suspicious loci in the simulations. Positive conditions were defined as
269 whether a true causal variant in a locus is 1) a lead PIP variant, 2) in 95% CS, and 3) in 99% CS. AUROC values were
270 shown in the labels. Black points represent the performance of our adopted metric, *i.e.*, whether a locus contains at
271 least one outlier variant ($P_{\text{DENTIST-S}} < 1.0 \times 10^{-4}$ and $r^2 > 0.6$). **d.** Calibration plot in the simulations under different PIP
272 thresholds. Calibration was measured as the mean PIP – fraction of true causal variants among variants above the
273 threshold. Shadows around the lines represent 95% confidence intervals. **e.** The fraction of variants in predicted
274 suspicious and non-suspicious loci under different PIP thresholds. Gray shadows in the panels **d,e** represent a PIP \leq
275 0.1 region as we excluded loci with maximum PIP ≤ 0.1 in the actual SLALOM analysis based on these panels.

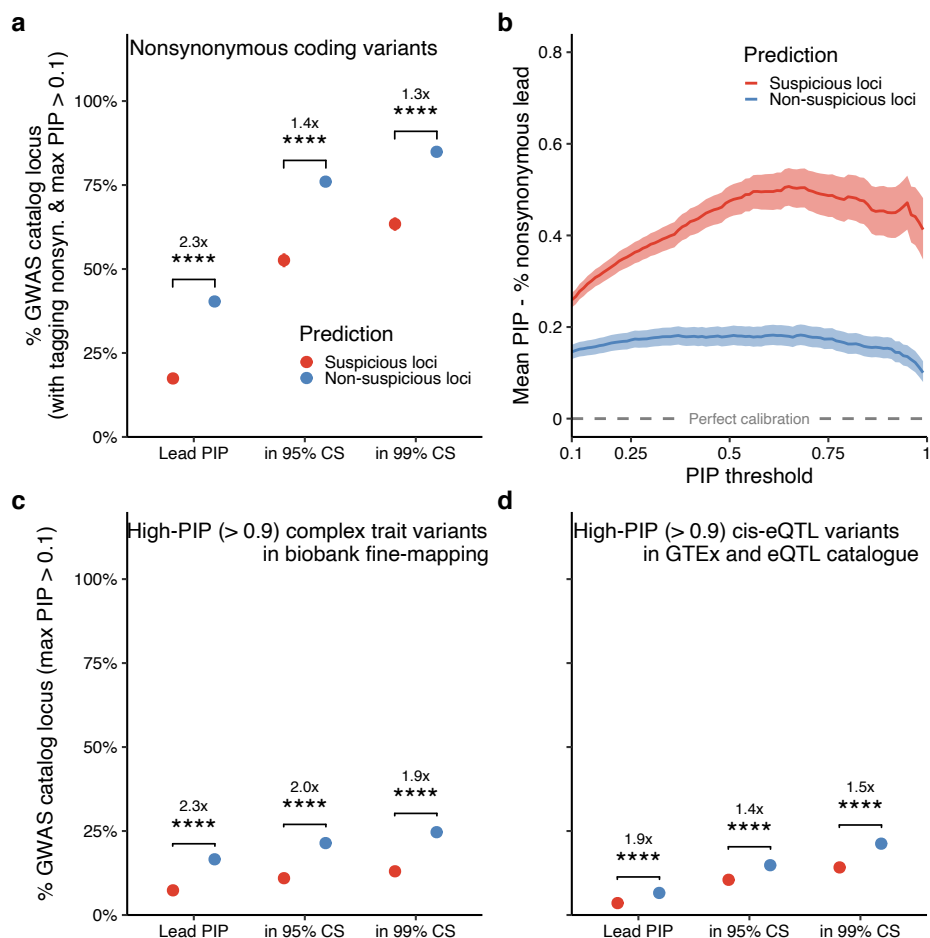
276 **Widespread suspicious loci for fine-mapping in existing meta-analysis summary** 277 **statistics**

278 Having assessed the performance of SLALOM in simulations, we applied SLALOM to 467 meta-
279 analysis summary statistics in the GWAS Catalog⁴⁸ that are publicly available with a sufficient
280 discovery sample size ($N > 10,000$; **Table S6; Methods**) to quantify the prevalence of suspicious
281 loci in existing studies. These summary statistics were mostly European ancestry-only meta-
282 analysis (63%), followed by multi-ancestry (31%), East Asian ancestry-only (3%), and African
283 ancestry-only (2%) meta-analyses. Across 467 summary statistics from 96 publications, we
284 identified 28,925 loci with maximum PIP > 0.1 (out of 35,864 genome-wide significant loci defined
285 based on 1 Mb window around lead variants; **Methods**) for SLALOM analysis, of which 8,137 loci
286 (28%) were predicted suspicious (**Table S7**).

287
288 To validate SLALOM performance in real data, we restricted our analysis to 6,065 loci that have
289 maximum PIP > 0.1 and that contain nonsynonymous coding variants (predicted loss-of-function
290 [pLoF] and missense) in LD with the lead variant ($r^2 > 0.6$). Given prior evidence^{16,17,44} that such
291 nonsynonymous variants are highly enriched for being causal, we tested the validity of our method
292 by whether they achieve the highest PIP in the locus (*i.e.*, successful fine-mapping) in suspicious
293 vs. non-suspicious loci (**Methods**). While 40% (1,557 / 3,860) of non-suspicious loci successfully
294 fine-mapped nonsynonymous variants, only 17% (384 / 2,205) of suspicious loci did,
295 demonstrating a significant depletion (2.3x) of successfully fine-mapped nonsynonymous variants
296 in suspicious loci (Fisher's exact $P = 3.6 \times 10^{-79}$; **Fig. 4a**). We also tested whether
297 nonsynonymous variants belonged to 95% and 99% CS and again observed significant depletion
298 (1.4x and 1.3x, respectively; Fisher's exact $P < 4.6 \times 10^{-100}$). In addition, when we used a more
299 stringent r^2 threshold (> 0.8) for selecting loci that contain nonsynonymous variants, we also
300 confirmed significant enrichment (Fisher's exact $P < 6.1 \times 10^{-65}$; **Fig. S10**). To quantify potential
301 fine-mapping miscalibration in the GWAS Catalog, we investigated the difference between mean
302 PIP for lead variants and fraction of lead variants that are nonsynonymous; assuming that
303 nonsynonymous variants in these loci are truly causal, this difference equals the difference
304 between the true and reported fraction of lead PIP variants that are causal. We observed
305 differences between 26–51% and 10–18% under different PIP thresholds in suspicious and non-
306 suspicious loci, respectively (**Fig. 4b**), marking 45% and 15% for high-PIP (> 0.9) variants.

307
308 We further assessed SLALOM performance in the GWAS Catalog meta-analyses by leveraging
309 high-PIP (> 0.9) complex trait and *cis*-eQTL variants that were rigorously fine-mapped^{16,17} in large-
310 scale biobanks (Biobank Japan [BBJ]⁵⁸, FinnGen²⁰, and UK Biobank [UKBB]¹⁹) and eQTL
311 resources (GTEx⁵⁹ v8 and eQTL Catalogue⁶⁰). Among the 27,713 loci analyzed by SLALOM
312 (maximum PIP > 0.1) that contain a lead variant that was included in biobank fine-mapping, 17%
313 (3,266 / 19,692) of the non-suspicious loci successfully fine-mapped one of the high-PIP GWAS
314 variants in biobank fine-mapping, whereas 7% (589 / 8,021) of suspicious loci did, showing a
315 significant depletion (2.3x) of the high-PIP complex trait variants in suspicious loci (Fisher's exact
316 $P = 4.6 \times 10^{-100}$; **Fig. 4c**). Similarly, among 26,901 loci analyzed by SLALOM that contain a lead
317 variant that was included in *cis*-eQTL fine-mapping, we found a significant depletion (1.9x) of the
318 high-PIP *cis*-eQTL variants in suspicious loci, where 7% (1,247 / 18,976) of non-suspicious loci
319 vs. 4% (281 / 7,925) of suspicious loci successfully fine-mapped one of the high-PIP *cis*-eQTL
320 variants (Fisher's exact $P = 2.6 \times 10^{-24}$; **Fig. 4d**). We observed the same significant depletions of
321 the high-PIP complex trait and *cis*-eQTL variants in suspicious loci that belonged to 95% and 99%
322 CS set (**Fig. 4c,d**).

323
324

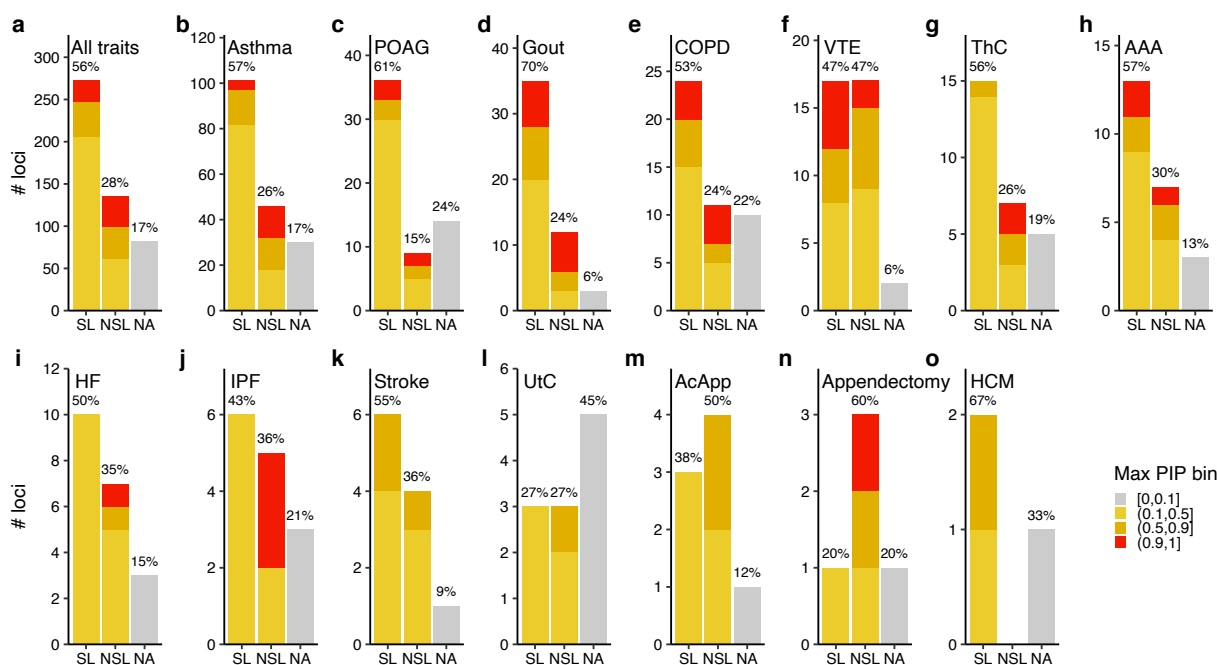


325
 326 **Fig. 4 | Evaluation of SLALOM performance in the GWAS Catalog summary statistics.** a,c,d. Depletion of likely
 327 causal variants in predicted suspicious loci. We evaluated whether (a) nonsynonymous coding variants (pLoF and
 328 missense), (c) high-PIP (> 0.9) complex trait variants in biobank fine-mapping, and (d) high-PIP (> 0.9) *cis*-eQTL
 329 variants in GTEx v8 and eQTL Catalogue were lead PIP variants, in 95% CS, or in 99% CS in suspicious vs. non-
 330 suspicious loci. Depletion was calculated by relative risk (*i.e.* a ratio of proportions; **Methods**). Error bars, invisible due
 331 to their small size, correspond to 95% confidence intervals using bootstrapping. Significance represents a Fisher's
 332 exact test *P*-value (*, *P* < 0.05; **, < 0.01; ***, < 0.001; ****, < 10⁻⁴). b. Plot of the estimated difference between true
 333 and reported proportion of causal variants in the loci tagging nonsynonymous variants (*r*² > 0.6 with the lead variants)
 334 in the GWAS Catalog under different PIP thresholds. Analogous to **Fig. 3b**, assuming nonsynonymous variants in these
 335 loci are truly causal, the mean PIP for lead variants minus the fraction of lead variants that are nonsynonymous above
 336 the threshold is equal to the difference between true and reported proportion of causal variants.
 337

338 Suspicious loci for fine-mapping in the GBMI summary statistics

339 Next, we applied SLALOM to meta-analysis summary statistics of 14 disease endpoints from the
 340 GBMI¹⁰. These summary statistics were generated from a meta-analysis of up to 1.8 million
 341 individuals in total across 18 biobanks for discovery, representing six different genetic ancestry
 342 groups of approximately 33,000 African, 18,000 Admixed American, 31,000 Central and South
 343 Asian, 341,000 East Asian, 1.4 million European, and 1,600 Middle Eastern individuals (**Table**
 344 **S8**). Among 489 genome-wide significant loci across the 14 traits (excluding the major
 345 histocompatibility complex [MHC] region, **Methods**), we found that 82 loci (17%) showed
 346 maximum PIP < 0.1, thus not being further considered by SLALOM. Of the remaining 407 loci
 347 with maximum PIP > 0.1, SLALOM identified that 272 loci (67%) were suspicious loci for fine-
 348 mapping (**Fig. 5a**; **Table S9**). The fraction of suspicious loci and their maximum PIP varied by
 349 trait, reflecting different levels of statistical power (e.g., sample sizes, heritability, and local LD
 350 structure) as well as inter-cohort heterogeneity (**Fig. 5b–o**).

351
 352 While the fraction of suspicious loci (67%) in the GBMI meta-analyses is higher than in the GWAS
 353 Catalog (28%), there might be multiple reasons for this discrepancy, including association
 354 significance, sample size, ancestral diversity, and study-specific QC criteria. For example, the
 355 GBMI summary statistics were generated from multi-ancestry, large-scale meta-analyses of
 356 median sample size of 1.4 million individuals across six ancestries, while 63% of the 467 summary
 357 statistics from the GWAS Catalog were only in European-ancestry studies and 83% had less than
 358 0.5 million discovery samples. Nonetheless, predicted suspicious loci for fine-mapping were
 359 prevalent in both the GWAS Catalog and the GBMI.
 360



361
 362 **Fig. 5 | SLALOM prediction results in the GBMI summary statistics.** For (a) all 14 traits and (b–o) individual traits,
 363 a number of predicted suspicious (SL), non-suspicious (NSL), and non-applicable (NA; maximum PIP < 0.1) loci were
 364 summarized. Individual traits are ordered by the total number of loci. Color represents the maximum PIP in a locus.
 365 Label represents the fraction of loci in each prediction category. AAA, abdominal aortic aneurysm. AcApp, acute
 366 appendicitis. COPD, chronic obstructive pulmonary disease. HCM, hypertrophic cardiomyopathy. HF, heart failure. IPF,
 367 idiopathic pulmonary fibrosis. POAG, primary open angle glaucoma. ThC, thyroid cancer. UtC, uterine cancer. VTE,
 368 venous thromboembolism.
 369

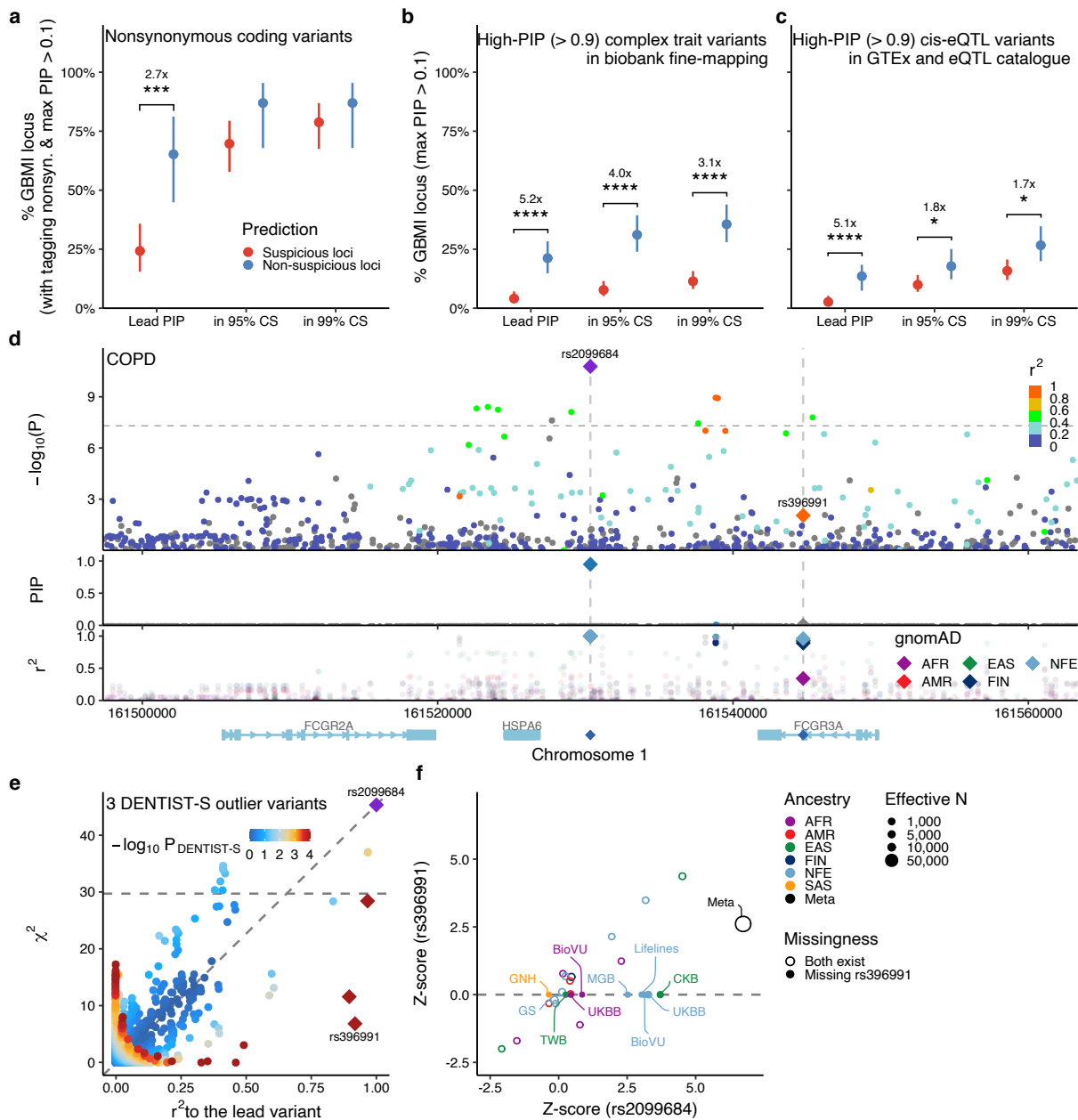
370 Using nonsynonymous (pLoF and missense) and high-PIP (> 0.9) complex trait and *cis*-eQTL
371 variants, we recapitulated a significant depletion of these likely causal variants in predicted
372 suspicious loci (2.7x, 5.2x, and 5.1x for nonsynonymous, high-PIP complex trait, and high-PIP
373 *cis*-eQTL variants being a lead PIP variant, respectively; Fisher's exact $P < 7.3 \times 10^{-4}$), confirming
374 our observation in the GWAS Catalog analysis (**Fig. 6a–c**).

375
376 In 15/23 non-suspicious loci harboring a nonsynonymous variant, the nonsynonymous variant
377 had the highest PIP. These included known missense variants such as rs116483731 (p.Arg20Gln)
378 in *SPDL1* for idiopathic pulmonary fibrosis (IPF)^{61,62} and rs28929474 (p.Glu366Lys) in *SERPINA1*
379 for chronic obstructive pulmonary disease (COPD)^{63,64}. In addition, we observed successful fine-
380 mapping in 2 novel loci for asthma, i) rs41286560 (p.Pro558Thr) in *RTL1*, a missense variant
381 known for decreasing height^{65,66} and ii) rs34187696 (p.Gly337Val) in *ZSCAN5A*, a known
382 missense variant for increasing monocyte count³⁰.

383
384 To characterize fine-mapping failures in suspicious loci, we examined suspicious loci in which a
385 nonsynonymous variant did not achieve the highest PIP. For example, the *FCGR2A/FCGR3A*
386 (1q23.3) locus for COPD contained a genome-wide significant lead intergenic variant rs2099684
387 ($P = 1.7 \times 10^{-11}$) which is in LD ($r^2 = 0.92$) with a missense variant rs396991 (p.Phe176Val) of
388 *FCGR3A* (**Fig. 6d**). This locus was not previously reported for COPD, but is known for
389 associations with autoimmune diseases (e.g., inflammatory bowel disease⁴⁴, rheumatoid
390 arthritis⁷, and systemic lupus erythematosus⁶⁷) and encodes the low-affinity human FC-gamma
391 receptors that bind to the Fc region of IgG and activate immune responses⁶⁸. Notably, this locus
392 contains copy number variations that contribute to the disease associations in addition to single-
393 nucleotide variants, which makes genotyping challenging^{68,69}. Despite strong LD with the lead
394 variant, rs396991 did not achieve genome-wide significance ($P = 9.1 \times 10^{-3}$), showing a significant
395 deviation from the expected association ($P_{\text{DENTIST-S}} = 5.3 \times 10^{-41}$; **Fig. 6e**). This is primarily due to
396 missingness of rs396991 in 8 biobanks out of 17 ($N_{\text{eff}} = 76,790$ and 36,781 for rs2099684 and
397 rs396991, respectively; **Fig. 6f**), which is caused by its absence from major imputation reference
398 panels (e.g., 1000GP⁴⁹, HRC⁵⁰, and UK10K⁷⁰) despite having a high MAF in every population
399 (MAF = 0.24–0.34 in African, admixed American, East Asian, European, and South Asian
400 populations of gnomAD⁵⁷).

401
402 Sample size imbalance across variants was pervasive in the GBMI meta-analyses⁷¹, and was
403 especially enriched in predicted suspicious loci—84% of suspicious loci vs. 24% of non-
404 suspicious loci showed a maximum/minimum effective sample size ratio > 2 among variants in
405 LD ($r^2 > 0.6$) with lead variants (a median ratio = 4.2 and 1.2 in suspicious and non-suspicious
406 loci, respectively; **Fig. S11**). These observations are consistent with our simulations,
407 recapitulating that sample size imbalance results in miscalibration for meta-analysis fine-mapping.
408 Notably, we observed a similar issue in other GBMI downstream analyses (e.g., polygenic risk
409 score [PRS]⁷¹ and drug discovery⁷²), where predictive performance improved significantly after
410 filtering out variants with maximum $N_{\text{eff}} < 50\%$. Although fine-mapping methods cannot simply
411 take this approach because it inevitably reduces calibration and recall by removing true causal
412 variants, other meta-analysis downstream analyses that primarily rely on polygenic signals rather
413 than individual variants should consider this filtering as an extra QC step.

414



415
416
417
418
419
420
421
422
423
424
425
426
427
428
429
430
431

Fig. 6 | Evaluation of SLALOM performance in the GBMI summary statistics. a–c. Similar to Fig. 4, we evaluated whether (a) nonsynonymous coding variants (pLoF and missense), (b) high-PIP (> 0.9) complex trait variants in biobank fine-mapping, and (c) high-PIP (> 0.9) cis-eQTL variants in GTEx v8 and eQTL Catalogue were lead PIP variants, in 95% CS, or in 99% CS in suspicious vs. non-suspicious loci. Depletion was calculated by relative risk (i.e. a ratio of proportions; **Methods**). Error bars correspond to 95% confidence intervals using bootstrapping. Significance represents a Fisher's exact test P -value (*, $P < 0.05$; **, $P < 0.01$; ***, $P < 0.001$; ****, $P < 10^{-4}$). d. Locuszoom plot of the 1q23.3 locus for COPD. The top panel shows a Manhattan plot, where the lead variant rs2099684 (purple diamond) and a missense variant rs396991 (orange diamond) are highlighted. Color represents r^2 values to the lead variant. Horizontal line represents a genome-wide significance threshold ($P = 5.0 \times 10^{-8}$). The middle panel shows PIP from ABF fine-mapping. Color represents whether variants belong to a 95% CS. The bottom panel shows r^2 values with the lead variant in gnomAD populations. e. A diagnosis plot showing r^2 values to the lead variant vs. marginal χ^2 . Color represents $-\log_{10} P_{\text{DENTIST-S}}$ values. Outlier variants with $P_{\text{DENTIST-S}} < 10^{-4}$ are depicted in red with a diamond shape. Diagonal line represents an expected marginal association. Horizontal line represents a genome-wide significance threshold. f. Z-scores of the lead variant (rs2099684) vs. the missense variant (rs396991) in the constituent cohorts of the meta-analysis. Open and closed circles represent whether both variants exist in a cohort or rs396991 is missing. Circle size corresponds to an effective sample size. Color represents genetic ancestry.

432 **Comparison of fine-mapping results between the GBMI meta-analyses and individual** 433 **biobanks**

434 Motivated by successful validation of SLALOM performance, we investigated whether fine-
435 mapping confidence and resolution were improved in the GBMI meta-analyses over individual
436 biobanks. To this end, we used our fine-mapping results^{16,17} of nine disease endpoints (asthma⁶⁴,
437 COPD⁶⁴, gout, heart failure⁷³, IPF⁶², primary open angle glaucoma⁷⁴, thyroid cancer, stroke⁷⁵, and
438 venous thromboembolism⁷⁶) in BBJ⁵⁸, FinnGen²⁰, and UKBB¹⁹ Europeans that also contributed to
439 the GBMI meta-analyses for the same traits.

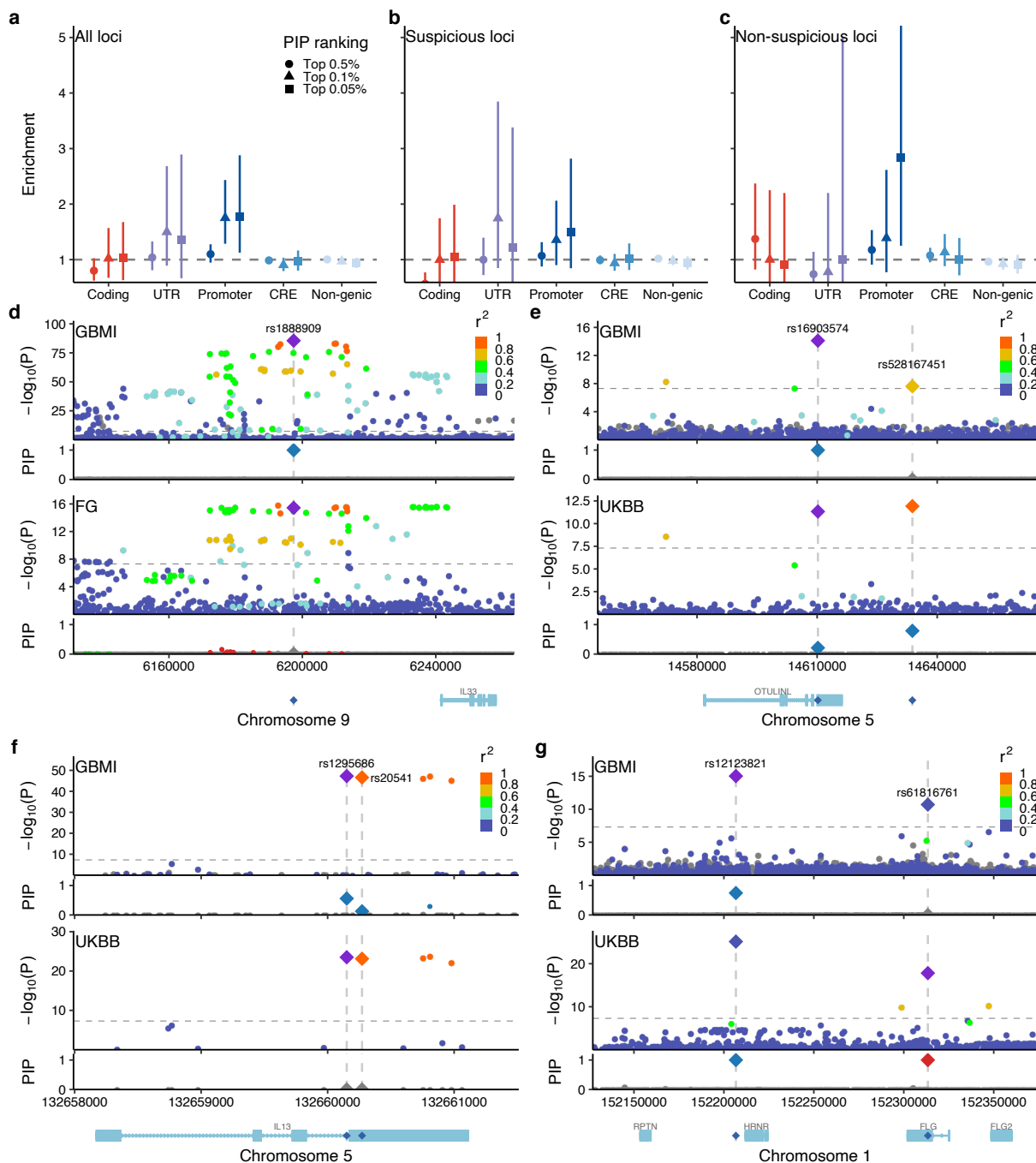
440
441 To perform an unbiased comparison of PIP between the GBMI meta-analysis and individual
442 biobanks, we investigated functional enrichment of fine-mapped variants based on top PIP
443 rankings in the GBMI and individual biobanks (top 0.5%, 0.1%, and 0.05% PIP variants in the
444 GBMI vs. maximum PIP across BBJ, FinnGen, and UKBB; **Methods**). Previous studies have
445 shown that high-PIP (> 0.9) complex trait variants are significantly enriched for well-known
446 functional categories, such as coding (pLoF, missense, and synonymous), 5'/3' UTR, promoter,
447 and *cis*-regulatory element (CRE) regions (DNase I hypersensitive sites [DHS] and H3K27ac)^{16,17}.
448 Using these functional categories, we found no significant enrichment of variants in the top PIP
449 rankings in the GBMI over individual biobanks (Fisher's exact $P > 0.05$; **Fig. 7a**) except for variants
450 in the promoter region (1.8x; Fisher's exact $P = 4.9 \times 10^{-4}$ for the top 0.1% PIP variants). We
451 observed similar trends regardless of whether variants were in suspicious or non-suspicious loci
452 (**Fig. 7b,c**). To examine patterns of increased and decreased PIP for individual variants, we also
453 calculated PIP difference between the GBMI and individual biobanks, defined as $\Delta\text{PIP} = \text{PIP}$
454 (GBMI) – maximum PIP across BBJ, FinnGen, and UKBB (**Fig. S12,13**). We investigated
455 functional enrichment based on ΔPIP bins and observed inconsistent enrichment results using
456 different ΔPIP thresholds (**Fig. S14**). Finally, to test whether fine-mapping resolution was
457 improved in the GBMI over individual biobanks, we compared the size of 95% CS after restricting
458 them to cases where a GBMI CS overlapped with an individual biobank CS from BBJ, FinnGen,
459 or UKBB (**Methods**). We observed the median 95% CS size of 2 and 2 in non-suspicious loci for
460 the GBMI and individual biobanks, respectively, and 5 and 14 in suspicious loci, respectively (**Fig.**
461 **S15**). The smaller credible set size in suspicious loci in GBMI could be due to improved resolution
462 or to increased miscalibration. These results provide limited evidence of overall fine-mapping
463 improvement in the GBMI meta-analyses over what is achievable by taking the best result from
464 individual biobanks.

465
466 Individual examples, however, provide insights into the types of fine-mapping differences that can
467 occur. To characterize the observed differences in fine-mapping confidence and resolution, we
468 further examined non-suspicious loci with $\Delta\text{PIP} > 0.5$ in asthma. In some cases, the increased
469 power and/or ancestral diversity of GBMI led to improved fine-mapping: for example, an intergenic
470 variant rs1888909 (~18 kb upstream of *IL33*) showed $\Delta\text{PIP} = 0.99$ (PIP = 1.0 and 0.008 in GBMI
471 and FinnGen, respectively; **Fig. 7d**), which was primarily owing to increased association
472 significance in a meta-analysis ($P = 3.0 \times 10^{-86}$, 7.4×10^{-2} , 3.6×10^{-16} , and 1.9×10^{-53} in GBMI,
473 BBJ, FinnGen, and UKBB Europeans, respectively) as well as a shorter LD length in the African
474 population than in the European population (LD length = 4 kb vs. 41 kb for variants with $r^2 > 0.6$
475 with rs1888909 in the African and European populations, respectively; $N_{\text{eff}} = 4,270$ for Africans in
476 the GBMI asthma meta-analysis; **Fig. S16**). This variant was also fine-mapped for eosinophil
477 count in UKBB Europeans (PIP = 1.0; $P = 1.3 \times 10^{-314}$)¹⁶ and was previously reported to regulate
478 *IL33* gene expression in human airway epithelial cells via allele-specific transcription factor
479 binding of OCT-1 (POU2F1)⁷⁷. Likewise, we observed a missense variant rs16903574
480 (p.Phe319Leu) in *OTULINL* showed $\Delta\text{PIP} = 0.79$ (PIP = 1.0 and 0.21 in GBMI and UKBB

481 Europeans, respectively; **Fig. 7e**) owing to improved association significance ($P = 7.7 \times 10^{-15}$ and
482 4.7×10^{-12} in GBMI and UKBB Europeans, respectively).

483
484 However, we also observed very high Δ PIP for variants that are not likely causal. For example,
485 we observed that an intronic variant rs1295686 in *IL13* showed Δ PIP = 0.56 (PIP = 0.56 and
486 0.0002 in GBMI and UKBB Europeans, respectively; **Fig. 7f**), despite having strong LD with a
487 nearby missense variant rs20541 (p.Gln144Arg; $r^2 = 0.96$ with rs1295686) which only showed
488 Δ PIP = 0.13 (PIP = 0.13 and 0.0001 in GBMI and UKBB Europeans, respectively). The missense
489 variant rs20541 showed PIP = 0.23 and 0.15 for a related allergic disease, atopic dermatitis, in
490 BBJ and FinnGen, respectively¹⁷, and was previously shown to induce STAT6 phosphorylation
491 and up-regulate CD23 expression in monocytes, promoting IgE synthesis⁷⁸. Although the GBMI
492 meta-analysis contributed to prioritizing these two variants (sum of PIP = 0.69 vs. 0.0003 in GBMI
493 and UKBB Europeans, respectively), the observed Δ PIP was higher for rs1295686 than for
494 rs20541.

495
496 While increasing sample size in meta-analysis improves association significance, we also found
497 negative Δ PIP due to losing the ability to model multiple causal variants. A stop-gained variant
498 rs61816761 (p.Arg501Ter) in *FLG* showed Δ PIP = -1.0 (PIP = 6.4×10^{-5} and 1.0 in GBMI and
499 UKBB Europeans, respectively; **Fig. 7g**), which was primarily owing to a nearby lead variant
500 rs12123821 (~17 kb downstream of *HRNR*; $r^2 = 0.0$ with rs61816761). This lead variant
501 rs12123821 showed greater significance than rs61816761 in GBMI ($P = 9.3 \times 10^{-16}$ and $2.0 \times 10^{-$
502 11 for rs12123821 and rs61816761, respectively) as well as in UKBB Europeans ($P = 7.1 \times 10^{-26}$
503 and 1.5×10^{-18}). While our biobank fine-mapping^{16,17} assigned PIP = 1.0 for both variants based
504 on multiple causal variant fine-mapping (*i.e.*, FINEMAP²¹ and SuSiE²³), our ABF fine-mapping in
505 the GBMI meta-analysis was only able to assign PIP = 0.74 for the lead variant rs12123821 due
506 to a single causal variant assumption. This recapitulates the importance of multiple causal variant
507 fine-mapping in complex trait fine-mapping^{16,17}—however, we note that multiple causal variant
508 fine-mapping with an external LD reference is extremely error-prone as previously reported^{14–16}.



509
 510 **Fig. 7 | Fine-mapping improvement and retrogression in the GBMI meta-analyses over individual biobanks.** a–
 511 c. Functional enrichment of variants in each functional category based on top PIP rankings in the GBMI and individual
 512 biobanks (maximum PIP of BBJ, FinnGen, and UKBB). Shape corresponds to top PIP ranking (top 0.5%, 0.1%, and
 513 0.05%). Enrichment was calculated by a relative risk (*i.e.* a ratio of proportions; **Methods**). Error bars correspond to
 514 95% confidence intervals using bootstrapping. **d–g**. Locuszoom plots for the same non-suspicious locus of asthma in
 515 the GBMI meta-analysis and an individual biobank (BBJ, FinnGen, or UKBB Europeans) that showed the highest PIP
 516 in our biobank fine-mapping. Colors in the Manhattan panels represent r^2 values to the lead variant. In the PIP panels,
 517 only fine-mapped variants in the 95% CS are colored, where the same colors are applied between the GBMI meta-
 518 analysis and an individual biobank based on merged CS as previously described. Horizontal line represents a genome-
 519 wide significance threshold ($P = 5.0 \times 10^{-8}$). **d**. rs1888909 for asthma in the GBMI and FinnGen. **e**. rs16903574 for
 520 asthma in the GBMI and UKBB Europeans. Nearby rs528167451 was also highlighted, which was in strong LD ($r^2 =$
 521 0.86) and in the same 95% CS in UKBB Europeans, but not in the GBMI ($r^2 = 0.67$).

522 GBMI and UKBB Europeans. A nearby missense, rs20541, showed lower PIP than rs1295686 despite having strong
523 LD ($r^2 = 0.96$). g. rs12123821 for asthma in the GBMI and UKBB Europeans. Nearby stop-gained rs61816761 was
524 independent of rs12123821 ($r^2 = 0.0$) and not fine-mapped in the GBMI due to a single causal variant assumption in
525 the ABF fine-mapping.
526

527 Discussion

528 In this study, we first demonstrated in simulations that meta-analysis fine-mapping is substantially
529 miscalibrated when constituent cohorts are heterogeneous in phenotyping, genotyping, and
530 imputation. To mitigate this issue, we developed SLALOM, a summary statistics-based QC
531 method for identifying suspicious loci in meta-analysis fine-mapping. Applying SLALOM to 14
532 disease endpoints from the GBMI meta-analyses¹⁰ as well as 467 summary statistics from the
533 GWAS Catalog⁴⁸, we observed widespread suspicious loci in meta-analysis summary statistics,
534 suggesting that meta-analysis fine-mapping is often miscalibrated in real data too. Indeed, we
535 demonstrated that the predicted suspicious loci were significantly depleted for having likely causal
536 variants as a lead PIP variant, such as nonsynonymous variants, high-PIP (> 0.9) GWAS and cis-
537 eQTL fine-mapped variants from our previous fine-mapping studies^{16,17}. Our method provides
538 better calibration in non-suspicious loci for meta-analysis fine-mapping, generating a more reliable
539 set of variants for further functional characterization.
540

541 We have found limited evidence of improved fine-mapping in the GBMI meta-analyses over
542 individual biobanks. A few empirical examples in this study as well as other previous
543 studies^{7,9,26,27,30} suggested that multi-ancestry, large-scale meta-analysis could have potential to
544 improve fine-mapping confidence and resolution owing to increased statistical power in
545 associations and differential LD pattern across ancestries. However, we have highlighted that the
546 observed improvement in PIP could be due to sample size imbalance in a locus, miscalibration,
547 and technical confoundings too, which further emphasizes the importance of careful investigation
548 of fine-mapped variants identified through meta-analysis fine-mapping. Given practical challenges
549 in data harmonization across different cohorts, a large-scale biobank with multiple ancestries
550 (e.g., UK Biobank¹⁹ and All of Us⁷⁹) would likely benefit the most from meta-analysis fine-mapping
551 across ancestries.
552

553 As high-confidence fine-mapping results in large-scale biobanks and molecular QTLs continue to
554 become available^{16,17,60}, we propose alternative approaches for prioritizing candidate causal
555 variants in a meta-analysis. First, these high-confidence fine-mapped variants have been a
556 valuable resource to conduct a “PheWAS”¹⁶ to match with associated variants in a meta-analysis,
557 which provides a narrower list of candidate variants assuming they would equally be functional
558 and causal in related complex traits or tissues/cell-types. Second, a traditional approach based
559 on tagging variants (e.g., $r^2 > 0.6$ with lead variants, or PICS⁸⁰ fine-mapping approach that only
560 relies on a lead variant and LD) can be still highly effective, especially for known functional
561 variants such as nonsynonymous coding variants. As we highlighted in this and previous³⁹
562 studies, potentially causal variants in strong LD with lead variants might not achieve genome-
563 wide significance because of missingness and heterogeneity.
564

565 While using an external LD reference for fine-mapping has been shown to be extremely error-
566 prone^{14–16}, we find here that it can be useful for flagging suspicious loci, even when it does not
567 perfectly represent the in-sample LD structure of the meta-analyzed individuals. However, our
568 use of external LD reference comes with several limitations. For example, due to the finite sample
569 size of external LD reference, rare or low-frequency variants have larger uncertainties around r^2
570 than common variants. Moreover, our r^2 values in a multi-ancestry meta-analysis are currently

571 approximated based on a sample-size-weighted average of r^2 across ancestries as previously
572 suggested⁸¹, but this can be different from actual r^2 . These uncertainties around r^2 affect SLALOM
573 prediction performance and should be modeled appropriately for further method development. On
574 the other hand, we find it challenging to use a LD reference when true causal variants are located
575 within a complex region (e.g., major histocompatibility complex [MHC]), or are entirely missing
576 from standard LD or imputation reference panels, especially for structural variants. These
577 limitations are not specific to meta-analysis fine-mapping, and separate fine-mapping methods
578 based on bespoke imputation references have been developed (e.g., HLA⁸², KIR⁸³, and variable
579 numbers of tandem repeats [VNTR]⁸⁴).

580
581 In addition, there are several methodological limitations of SLALOM. First, our simulations only
582 include one causal variant per locus. Although additional independent causal variants would not
583 affect SLALOM precision (but decrease recall), multiple *correlated* causal variants in a locus
584 would violate SLALOM assumptions and could lead to some DENTIST-S outliers that are not due
585 to heterogeneity or missingness but rather simply a product of tagging multiple causal variants in
586 LD. In fact, our previous studies have illustrated infrequent but non-zero presence of such
587 correlated causal variants in complex traits^{16,17}. Second, SLALOM prediction is not perfect.
588 Although fine-mapping calibration is certainly better in non-suspicious vs. suspicious loci,
589 SLALOM has low precision, and we still observe some miscalibration in non-suspicious loci.
590 Optimal thresholds for SLALOM prediction might be different for other datasets. Third, SLALOM
591 does not model effect size heterogeneity. Although SLALOM is able to detect suspicious loci due
592 to effect size heterogeneity as the method is agnostic to the source of heterogeneity, methods
593 which model effect size heterogeneity, such as MR-MEGA⁸⁵, could improve SLALOM
594 performance. Finally, SLALOM is a per-locus QC method and does not calibrate per-variant PIPs.
595 Further methodological development that properly models heterogeneity, missingness, sample
596 size imbalance, multiple causal variants, and LD uncertainty across multiple cohorts and
597 ancestries is needed to refine per-variant calibration and recall in meta-analysis fine-mapping.

598
599 We have found evidence in our simulations and real data of severe miscalibration of fine-mapping
600 results from GWAS meta-analysis; for example, we estimate that the difference between true and
601 reported proportion of causal variants is 20% and 45% for high-PIP (> 0.9) variants in suspicious
602 loci from the simulations and the GWAS Catalog, respectively. Our SLALOM method helps to
603 exclude spurious results from meta-analysis fine-mapping; however, even fine-mapping results in
604 SLALOM-predicted “non-suspicious” loci remain somewhat miscalibrated, showing estimated
605 differences between true and reported proportion of causal variants of 4% and 15% for high-PIP
606 variants in the simulations and the GWAS Catalog, respectively. We thus urge extreme caution
607 when interpreting PIPs computed from meta-analyses until improved methods are available. We
608 recommend that researchers looking to identify likely causal variants employ complete
609 synchronization of study design, case/control ascertainment, genomic profiling, and analytical
610 pipeline, or rely more heavily on functional annotations, biobank fine-mapping, or molecular QTLs.
611

612 **Acknowledgements**

613 We acknowledge all the participants and researchers of the 23 biobanks that have contributed to
614 the GBMI. Biobank-specific acknowledgements are included in the **Supplementary Note**. We
615 thank H. Huang, A.R. Martin, B.M. Neale, Y. Okada, K. Tsoo, J.C. Ulirsch, Y. Wang, and all the
616 members of Finucane and Daly labs for their helpful feedback. M.K. was supported by a Nakajima
617 Foundation Fellowship and the Masason Foundation. H.K.F. was funded by NIH grant DP5
618 OD024582.

619 **Author contributions**

620 M.K., M.J.D, and H.K.F. designed the study. M.K., R.E. and W.Z. performed analyses. H.K.F
621 supervised this work. H.K.F. and M.K. obtained funding. M.K., R.E., M.J.D., and H.K.F. wrote the
622 manuscript with input from all authors.

623 **Competing interests**

624 M.J.D. is a founder of Maze Therapeutics. All other authors declare no competing interests.

625 **STAR Methods**

626 **Resource availability**

627 **Lead contact**

628 Further information and requests for resources and data should be directed to and will be fulfilled
629 by the lead contact, Masahiro Kanai (mkanai@broadinstitute.org).

630 **Materials availability**

631 This study did not generate new unique reagents.

632 **Data and code availability**

633 The GBMI summary statistics for the 14 endpoints are publicly available and are browserble at
634 the GBMI PheWeb website (<http://results.globalbiobankmeta.org/>). Example outputs from the
635 meta-analysis fine-mapping simulation pipeline have been deposited at Harvard Dataverse. All
636 original code has been deposited at Zenodo and is publicly available as of the date of publication.
637 DOIs and links are listed in the key resources table. Any additional information required to
638 reanalyze the data reported in this paper is available from the lead contact upon request.

639 **Method details**

640 **Meta-analysis fine-mapping simulation**

641 To benchmark fine-mapping performance in meta-analysis, we simulated a large-scale, realistic
642 GWAS meta-analysis and performed fine-mapping under different scenarios. An overview of our
643 simulation pipeline is summarized in **Fig. S2**.

644 *Simulated true genotype*

645 Using HAPGEN2⁸⁷ with the 1000 Genomes Project Phase 3 reference⁴⁹, we simulated “true”
646 genotypes of chromosome 3 for multiple independent cohorts from African, East Asian, and
647 European ancestries. For each independent cohort from a given ancestry, we simulated 10,000
648 individuals each using the default parameters, with an ancestry-specific effective population size
649 set to 17,469, 14,269, and 11,418 for Africans, East Asians, and Europeans, respectively, as
650 recommended⁸⁷. To mimic sample size imbalance of different ancestries in the current meta-
651 analyses, we simulated 10 independent European cohorts, 1 African cohort, and 1 East Asian
652 cohort.

653
654 To restrict our analysis to unrelated samples, we computed sample relatedness based on KING
655 kinship coefficients⁸⁸ using PLINK 2.0 (ref. ⁸⁹) and removed monozygotic twins, duplicated
656 individuals, or first-degree relatives with the coefficient threshold of 0.177. The detailed sample
657 sizes of unrelated individuals for each cohort is summarized in **Table S1**.

658 *Genotyping and imputation*

659 To simulate realistic genotyping and imputation procedures, we first virtually genotyped each
660 cohort by restricting variants to those that are available on different genotyping arrays. We
661 selected three major genotyping arrays from Illumina, Inc. (Omni2.5, Multi-Ethnic Global Array
662 [MEGA], and Global Screening Array [GSA]) that have different densities of genotyping probes
663 (**Table S2**). For each cohort, we created three virtually genotyped datasets by retaining variants
664 that are genotyped on each array. For the sake of simplicity, we assumed no genotyping errors
665 occurred between true genotypes and virtually genotyped data—however, in practice, genotyping
666 error is one of the major sources of unexpected confounding (e.g., see recent discussions
667 here^{90,91}) and should be treated carefully.

668
669 For each pair of cohort and genotyping array, we then imputed missing variants using different
670 imputation reference panels. We used the Michigan Imputation Server
671 (<https://imputationserver.sph.umich.edu/>)⁹² and the TOPMed Imputation Server
672 (<https://imputation.biodatacatalyst.nhlbi.nih.gov/>)⁵¹ with the default parameters, using three
673 publicly available reference panels: the 1000 Genomes Project Phase 3 (version 5; $n = 2,504$;
674 1000GP3)⁴⁹, the Haplotype Reference Consortium (version r1.1; $n = 32,470$; HRC)⁵⁰, and the
675 TOPMed (version R2; $n = 97,256$)⁵¹. Briefly, for each input, the imputation server created chunks
676 of 20 Mb, applied the standard QC, pre-phased each chunk with Eagle2 (ref. ⁹³), and imputed
677 non-genotyped variants using a specified reference panel with Minimac4
678 (<https://genome.sph.umich.edu/wiki/Minimac4>). The detailed documentation of the imputation
679 pipeline is available on the Michigan and TOPMed websites and has been described elsewhere⁹².

680
681 We applied post-imputation QC by only keeping variants with $MAF > 0.001$ and imputation $Rsq >$
682 0.6 . Because the TOPMed panel is based on GRCh38 while the 1000GP3 and the HRC panels
683 are on GRCh37, we lifted over TOPMed variants from GRCh38 to GRCh37 to meta-analyze with
684 other cohorts. We excluded any variants which were lifted over to different chromosomes or for
685 which the conversion failed. The number of virtually genotyped and imputed variants for each
686 combination of cohort, genotyping array, and imputation panel is summarized in **Table S3**.

687 *True phenotype*

688 We simulated 300 true phenotypes that resemble observed complex trait genetic architecture and
689 phenotypic heterogeneity across cohorts. Based on previous literature, we set parameters as
690 follows: 1) 50% of 1 Mb loci contain a true causal variant⁹⁴; 2) probability of being causal is

691 proportional to functional enrichments of variant consequences (pLoF, missense, synonymous,
692 5'/3' UTR, promoter, cis-regulatory region, and non-genic) for fine-mapped variants as estimated
693 in a previous complex trait fine-mapping study¹⁷; 3) per-allele causal effect sizes have a variance
694 proportional to $[2p(1-p)]^\alpha$ where p represents a maximum MAF across the three ancestries
695 (AFR, EAS, and EUR) and α is set to be -0.38 (ref. ⁵²); and 4) total SNP-heritability h_g^2 for
696 chromosome 3 equals 0.03 (ref. ⁵³). For the sake of simplicity, we randomly draw a single true
697 causal variant per locus because ABF assumes a single causal variant^{31,32}. We draw true causal
698 variants from 1,150,893 non-ambiguous single-nucleotide variants in 1000GP3 that showed MAF
699 > 0.01 in at least one of the three ancestries (AFR, EAS, or EUR) and were not located within
700 conversion-unstable positions (CUP)⁵⁴ between the human genome builds GRCh37 and
701 GRCh38. To mimic phenotypic heterogeneity across cohorts in real-world meta-analysis (due to
702 e.g., different ascertainment, measurement error, or true effect size heterogeneity), we introduced
703 cross-cohort genetic correlation of true effect sizes r_g which is set to be one of 1, 0.9, or 0.5. For
704 a true causal variant j , true causal effect sizes β_j across cohorts were randomly drawn from $\beta_j \sim$
705 $MVN(0, \Sigma)$ where diagonal elements of Σ were set to be $\sigma_g^2 \cdot [2p(1-p)]^\alpha$ and off-diagonal
706 elements of Σ were set to be $r_g \cdot \sigma_g^2 \cdot [2p(1-p)]^\alpha$. σ_g^2 was determined by $\sigma_g^2 = h_g^2 /$
707 $\sum_j [2p(1-p)]^{1+\alpha}$. For each cohort, true phenotype y was computed via $y = X\beta + \varepsilon$ where X
708 is the above true genotype matrix from HAPGEN2 and $\varepsilon_i \sim N(0, 1 - \sigma_g^2)$ i.i.d. We simulated 100
709 true phenotypes for each of $r_g = 1, 0.9, \text{ and } 0.5$, respectively.

710 GWAS

711 For each combination of phenotype, cohort, genotyping chip, and imputation panel, we conducted
712 GWAS via a standard linear regression as implemented in PLINK 2.0 using imputed dosages. For
713 covariates, we included top 10 principal components that were calculated based on true
714 genotypes after restricting to unrelated samples. We only used LD-pruned variants with MAF $>$
715 0.01 for PCA.

716 Meta-analysis

717 To simulate meta-analyses that resemble real-world settings, we generated multiple
718 *configurations* of the above GWAS results to meta-analyze across 10 independent cohorts.
719 Briefly, we chose configurations based on the following settings: 1) 10 EUR cohorts are genotyped
720 and imputed using the same genotyping array (one of GSA, MEGA, or Omni2.5) and the same
721 imputation panel (one of 1000GP3, HRC, TOPMed, or TOPMed-liftover); 2) 10 cohorts consisting
722 of multiple ancestries (9 EUR + 1 AFR/EAS cohorts or 8 EUR + 1 AFR + 1 EAS cohorts), with all
723 cohorts genotyped and imputed using the same array (Omni2.5) and the same panel (1000GP3);
724 3) 10 EUR or multi-ancestry cohorts are genotyped using the same array (Omni2.5) but imputed
725 using different panels across cohorts; 4) 10 EUR or multi-ancestry cohorts are imputed using the
726 same panel (1000GP3) but genotyped using different arrays across cohorts; 5) 10 EUR or multi-
727 ancestry cohorts are genotyped and imputed using different arrays and panels across cohorts.
728 For settings 3–5, we randomly draw a combination of a genotyping array and an imputation panel
729 for each cohort five times each for 10 EUR and multi-ancestry cohorts. In total, we generated 45
730 configurations as summarized in **Table S4**.

731
732 For each configuration, we conducted a fixed-effect meta-analysis based on inverse-variance
733 weighted betas and standard errors using a modified version of PLINK 1.9
734 (https://github.com/mkanai/plink-ng/tree/add_se_meta).

735 *Fine-mapping*

736 For each meta-analysis, we defined fine-mapping regions based on a 1 Mb window around each
737 genome-wide significant lead variant and applied ABF^{31,32} using prior effect size variance of $\sigma_0^2 =$
738 0.04. We set a prior variance of effect size to be 0.04 which was taken from Wakefield et al.³¹ and
739 is commonly used in meta-analysis fine-mapping studies^{2,7}. We computed posterior inclusion
740 probability (PIP) and 95% credible set (CS) for each locus and evaluated whether true causal
741 variants were correctly fine-mapped.

742 **The SLALOM method**

743 SLALOM takes GWAS summary statistics and external LD reference as input and predicts
744 whether a locus is suspicious for fine-mapping. SLALOM consists of the following three steps:

745 *Locus definition*

746 Consistent with common fine-mapping region definition, we defined loci based on a 1 Mb window
747 around each genome-wide significant lead variant and merged them if they overlapped. We
748 excluded the major histocompatibility complex (MHC) region (chr 6: 25-36 Mb) from analysis due
749 to extensive LD structure in the region.

750 *DENTIST-S outlier detection*

751 For each variant in a locus, we computed DENTIST-S statistics using equation (1) based on the
752 assumption of a single causal variant. DENTIST-S P-values ($P_{\text{DENTIST-S}}$) were computed using the
753 χ^2 distribution with 1 degree of freedom. We applied ABF^{31,32} using prior effect size variance of
754 $\sigma_0^2 = 0.04$ and used the lead PIP variant (the variant with the highest PIP) as an approximation of
755 the causal variant in the locus. To retrieve correlation r among the variants, we used publicly
756 available LD matrices from gnomAD⁵⁷ v2 as external LD reference for African, Admixed American,
757 East Asian, Finnish, and non-Finnish European populations. When multiple populations exist, we
758 computed a sample-size-weighted average of r^2 using per-variant sample sizes for each
759 population as previously suggested⁸¹. We excluded variants without r^2 available in gnomAD from
760 the analysis. Since gnomAD v2 LD matrices are based on the human genome assembly GRCh37,
761 variants were lifted over to GRCh38 if the input summary statistics were based on GRCh38.

762
763 We determined DENTIST-S outlier variants using two thresholds: 1) $r^2 > \rho$ to the lead and 2)
764 $P_{\text{DENTIST-S}} < \tau$. The thresholds ρ and τ were set to $\rho = 0.6$ and $\tau = 1.0 \times 10^{-4}$ based on the training
765 in simulations as described below.

766 *Suspicious loci prediction*

767 We predicted whether a locus is suspicious or non-suspicious for fine-mapping based on the
768 number of DENTIST-S outlier variants in the locus $> \kappa$. To determine the best-performing
769 thresholds (ρ , τ , and κ), we used loci with maximum PIP > 0.9 in the simulations for training.
770 Positive conditions were defined as whether a true causal variant in a locus is 1) a lead PIP
771 variant, 2) in 95% CS, and 3) in 99% CS. We computed AUROC across different thresholds ($\rho =$
772 0, 0.1, 0.2, ..., 0.9; $-\log_{10} \tau = 0, 0.5, 1, \dots, 10$; and $\kappa = 0, 1, 2, \dots$) and chose $\rho = 0.6$, $\tau = 1.0 \times 10^{-4}$,
773 and $\kappa = 0$ that showed the highest AUROC for all the aforementioned positive conditions. Using
774 all the loci in the simulations, we then evaluated fine-mapping miscalibration (defined as mean
775 PIP – fraction of true causal variants) at different PIP thresholds in suspicious and non-suspicious
776 loci and decided to only apply SLALOM to loci with maximum PIP > 0.1 owing to relatively lower
777 miscalibration and specificity of SLALOM at lower PIP thresholds.

778 **GWAS Catalog analysis**

779 We retrieved full GWAS summary statistics publicly available on the GWAS Catalog⁴⁸. Out of
780 33,052 studies from 5,553 publications registered at the GWAS Catalog (as of January 12, 2022),
781 we selected 467 studies from 96 publications that have 1) full harmonized summary statistics
782 preprocessed by the GWAS Catalog with non-missing variant ID, marginal beta, and standard
783 error columns, 2) a discovery sample size of more than 10,000 individuals, 3) African (including
784 African American, Afro-Caribbean, and Sub-Saharan African), admixed American (Hispanic and
785 Latin American), East Asian, or European samples based on their broad ancestral category
786 metadata, 4) at least one genome-wide significant association ($P < 5.0 \times 10^{-8}$), and 5) our manual
787 annotation as a meta-analysis rather than a single-cohort study (**Table S6**). We applied SLALOM
788 to the 467 summary statistics and identified 35,864 genome-wide significant loci (based on 1 Mb
789 window around lead variants), of which 28,925 loci with maximum PIP > 0.1 were further classified
790 into suspicious and non-suspicious loci. Since per-variant sample sizes were not available, we
791 used overall sample sizes of each ancestry (African, Admixed American, East Asian, and
792 European) to calculate the weighted-average of r^2 . All the variants were harmonized into the
793 human genome assembly GRCh38 by the GWAS Catalog.

794 **GBMI analysis**

795 We used meta-analysis summary statistics of 14 disease endpoints from the GBMI (**Table S8**).
796 These meta-analyses were conducted using up to 1.8 million individuals across 18 biobanks for
797 discovery, representing six different genetic ancestry groups (approximately 33,000 African,
798 18,000 Admixed American, 31,000 Central and South Asian, 341,000 East Asian, 1.4 million
799 European, and 1,600 Middle Eastern individuals). Detailed procedures of the GBMI meta-
800 analyses were described in the GBMI flagship publication¹⁰.

801
802 Across the 14 summary statistics, we used 489 out of 500 genome-wide significant loci ($P < 5.0$
803 $\times 10^{-8}$; 1 Mb window around each lead variant, as defined in the GBMI flagship publication¹⁰),
804 excluding 11 loci that overlap with the MHC region. We applied SLALOM to 422 loci with maximum
805 PIP > 0.1 based on the ABF fine-mapping and predicted whether they were suspicious or non-
806 suspicious for fine-mapping. We used per-variant sample sizes of each ancestry (African,
807 Admixed American, East Asian, Finnish, and non-Finnish European) to calculate the weighted-
808 average of r^2 . Since gnomAD LD matrices were not available for Central and South Asian and
809 Middle Eastern, we did not use their sample sizes for the calculation. All the variants were
810 processed on the human genome assembly GRCh38.

811 **Fine-mapping results of complex traits and *cis*-eQTL**

812 We retrieved our previous fine-mapping results for 1) complex traits in large-scale biobanks
813 (BBJ⁵⁸, FinnGen²⁰, and UKBB¹⁹ Europeans)^{16,17} and 2) *cis*-eQTLs in GTEx⁵⁹ v8 and eQTL
814 Catalogue⁶⁰. Briefly, we conducted multiple-causal-variant fine-mapping (FINEMAP^{21,22} and
815 SuSiE²³) of complex trait GWAS (# unique traits = 148) and *cis*-eQTL gene expression (# unique
816 tissues/cell-types = 69) using summary statistics and in-sample LD. Detailed fine-mapping
817 methods are described elsewhere^{16,17}.

818
819 In this study, we collected 1) high-PIP GWAS variants that achieved PIP > 0.9 for any traits in any
820 biobank and 2) high-PIP *cis*-eQTL variants that achieved PIP > 0.9 for any gene expression in
821 any tissues/cell-types. All the variants were originally processed on the human genome assembly
822 GRCh37 and lifted over to the GRCh38 for comparison.

823 *Additional fine-mapping results*

824 To compare with the GBMI meta-analyses, we additionally conducted multi-causal-variant fine-
825 mapping of four additional endpoints (gout, heart failure, thyroid cancer, and venous
826 thromboembolism) that were not fine-mapped in our previous study^{16,17}. We used exactly the
827 same fine-mapping pipeline (FINEMAP^{21,22} and SuSiE²³) as described previously^{16,17}. For UKBB
828 Europeans, to use the exact same samples that contributed to the GBMI, we used individuals of
829 European ancestry ($n = 420,531$) as defined in the Pan-UKBB project
830 (<https://pan.ukbb.broadinstitute.org>), instead of those of “white British ancestry” ($n = 361,194$)
831 used in our previous study^{16,17}.

832 **Enrichment analysis of likely causal variants**

833 To validate SLALOM performance, we asked whether suspicious and non-suspicious loci were
834 enriched for having likely causal variants as a lead PIP variant, and for containing them in the
835 95% and 99% CS. We defined likely causal variants using 1) nonsynonymous coding variants,
836 *i.e.*, pLoF and missense variants annotated⁹⁵ by the Ensembl Variant Effect Predictor (VEP) v101
837 (using GRCh38 and GENCODE v35), 2) the high-PIP (> 0.9) complex trait fine-mapped variants,
838 and 3) the high-PIP (> 0.9) *cis*-eQTL fine-mapped variants from our previous studies as described
839 above.

840
841 We estimated enrichment for suspicious and non-suspicious loci as a relative risk (*i.e.*, a ratio of
842 proportion of variants) between being in suspicious/non-suspicious loci and having the annotated
843 likely causal variants as a lead PIP variant (or containing them in the 95% or 99% CS). That is, a
844 relative risk = (proportion of non-suspicious loci having the annotated variants as a lead PIP
845 variant) / (proportion of suspicious loci having the annotated variants as a lead PIP variant). We
846 computed 95% confidence intervals using bootstrapping.

847 **Comparison of fine-mapping results between the GBMI and individual biobanks**

848 To directly compare with fine-mapping results from the GBMI meta-analyses, we used our fine-
849 mapping results of nine disease endpoints (asthma⁶⁴, COPD⁶⁴, gout, heart failure⁷³, IPF⁶², primary
850 open angle glaucoma⁷⁴, thyroid cancer, stroke⁷⁵, and venous thromboembolism⁷⁶) in BBJ⁵⁸,
851 FinnGen²⁰, and UKBB¹⁹ Europeans that were also part of the GBMI meta-analyses for the same
852 traits. For comparison, we computed the maximum PIP for each variant and the minimum size of
853 95% CS across BBJ, FinnGen, and UKBB. We restricted the 95% CS in biobanks to those that
854 contain the lead variants from the GBMI. We defined the PIP difference between the GBMI and
855 individual biobanks as $\Delta\text{PIP} = \text{PIP}(\text{GBMI}) - \text{the maximum PIP across the biobanks}$.

856
857 We conducted functional enrichment analysis to compare between the GBMI meta-analysis and
858 individual biobanks because unbiased comparison of PIP requires conditioning on likely causal
859 variants independent of the fine-mapping results, and functional annotations have been shown to
860 be enriched for causal variants. Using functional categories (coding [pLoF, missense, and
861 synonymous], 5'/3' UTR, promoter, and CRE) from our previous study^{16,17}, we estimated
862 functional enrichments of variants in each functional category based on 1) top PIP rankings and
863 2) ΔPIP bins. Since fine-mapping PIP in the GBMI meta-analysis can be miscalibrated, we
864 performed a comparison based on top PIP rankings to assess whether the ordering given by
865 GBMI PIPs is more informative than the ordering given by the biobanks. For the top PIP rankings,
866 we took the top 0.5%, 0.1%, and 0.05% variants based on the PIP rankings in the GBMI and
867 individual biobanks. We computed enrichment as a relative risk = (proportion of top X% PIP
868 variants in the GBMI that are in the annotation) / (proportion of top X% PIP variants in the
869 individual biobanks that are in the annotation). For ΔPIP bins, we defined three bins using different

870 thresholds ($\theta = 0.01, 0.05, \text{ and } 0.1$): 1) decreased PIP bin, $\Delta\text{PIP} < -\theta$, 2) null bin, $-\theta \leq \Delta\text{PIP} \leq \theta$,
871 and 3) increased PIP bin, $\theta < \Delta\text{PIP}$. We computed enrichment as a relative risk = (proportion of
872 variants in the decreased/increased PIP bin that are in the annotation) / (proportion of variants in
873 the null PIP bin). We combined coding, UTR, and promoter categories for this analysis due to the
874 limited number of variants for each bin.

875 References

- 876 1. Evangelou, E. & Ioannidis, J. P. a. Meta-analysis methods for genome-wide association
877 studies and beyond. *Nat. Rev. Genet.* **14**, 379–389 (2013).
- 878 2. Mahajan, A. *et al.* Fine-mapping type 2 diabetes loci to single-variant resolution using high-
879 density imputation and islet-specific epigenome maps. *Nat. Genet.* **50**, 1505–1513 (2018).
- 880 3. Spracklen, C. N. *et al.* Identification of type 2 diabetes loci in 433,540 East Asian
881 individuals. *Nature* **582**, 240–245 (2020).
- 882 4. Ripke, S. *et al.* Biological insights from 108 schizophrenia-associated genetic loci. *Nature*
883 **511**, 421–427 (2014).
- 884 5. The Schizophrenia Working Group of the Psychiatric Genomics Consortium, Ripke, S.,
885 Walters, J. T. R. & O'Donovan, M. C. Mapping genomic loci prioritises genes and implicates
886 synaptic biology in schizophrenia. *bioRxiv* (2020) doi:10.1101/2020.09.12.20192922.
- 887 6. Okada, Y. *et al.* Genetics of rheumatoid arthritis contributes to biology and drug discovery.
888 *Nature* **506**, 376–381 (2014).
- 889 7. Ishigaki, K. *et al.* Trans-ancestry genome-wide association study identifies novel genetic
890 mechanisms in rheumatoid arthritis. *bioRxiv* (2021) doi:10.1101/2021.12.01.21267132.
- 891 8. Locke, A. E. *et al.* Genetic studies of body mass index yield new insights for obesity
892 biology. *Nature* **518**, 197–206 (2015).
- 893 9. Graham, S. E. *et al.* The power of genetic diversity in genome-wide association studies of
894 lipids. *Nature* **600**, 675–679 (2021).
- 895 10. Zhou, W. *et al.* Global Biobank Meta-analysis Initiative: powering genetic discovery across
896 human diseases. *bioRxiv* (2021) doi:10.1101/2021.11.19.21266436.
- 897 11. Visscher, P. M. *et al.* 10 Years of GWAS Discovery: Biology, Function, and Translation.
898 *Am. J. Hum. Genet.* **101**, 5–22 (2017).
- 899 12. Shendure, J., Findlay, G. M. & Snyder, M. W. Genomic Medicine-Progress, Pitfalls, and
900 Promise. *Cell* **177**, 45–57 (2019).
- 901 13. Schaid, D. J., Chen, W. & Larson, N. B. From genome-wide associations to candidate
902 causal variants by statistical fine-mapping. *Nat. Rev. Genet.* **19**, 491–504 (2018).
- 903 14. Ulirsch, J. C. *et al.* Interrogation of human hematopoiesis at single-cell and single-variant
904 resolution. *Nat. Genet.* **51**, 683–693 (2019).
- 905 15. Weissbrod, O. *et al.* Functionally informed fine-mapping and polygenic localization of
906 complex trait heritability. *Nat. Genet.* **52**, 1355–1363 (2020).
- 907 16. Ulirsch, J. C. & Kanai, M. An annotated atlas of causal variants underlying complex traits
908 and gene expression. *Under review*.
- 909 17. Kanai, M. *et al.* Insights from complex trait fine-mapping across diverse populations.
910 *medRxiv* (2021) doi:10.1101/2021.09.03.21262975.
- 911 18. Nagai, A. *et al.* Overview of the BioBank Japan Project: Study design and profile. *J.*
912 *Epidemiol.* **27**, S2–S8 (2017).
- 913 19. Bycroft, C. *et al.* The UK Biobank resource with deep phenotyping and genomic data.
914 *Nature* **562**, 203–209 (2018).
- 915 20. Kurki, M. I. *et al.* FinnGen: Unique genetic insights from combining isolated population and
916 national health register data. *bioRxiv* (2022) doi:10.1101/2022.03.03.22271360.
- 917 21. Benner, C. *et al.* FINEMAP: Efficient variable selection using summary data from genome-

- 918 wide association studies. *Bioinformatics* **32**, 1493–1501 (2016).
- 919 22. Benner, C., Havulinna, A. S., Salomaa, V., Ripatti, S. & Pirinen, M. Refining fine-mapping:
920 effect sizes and regional heritability. *bioRxiv* 318618 (2018) doi:10.1101/318618.
- 921 23. Wang, G., Sarkar, A., Carbonetto, P. & Stephens, M. A simple new approach to variable
922 selection in regression, with application to genetic fine mapping. *J. R. Stat. Soc. Series B*
923 *Stat. Methodol.* **82**, 1273–1300 (2020).
- 924 24. Onengut-Gumuscu, S. *et al.* Fine mapping of type 1 diabetes susceptibility loci and
925 evidence for colocalization of causal variants with lymphoid gene enhancers. *Nat. Genet.*
926 **47**, 381–386 (2015).
- 927 25. Levey, D. F. *et al.* Bi-ancestral depression GWAS in the Million Veteran Program and meta-
928 analysis in >1.2 million individuals highlight new therapeutic directions. *Nat. Neurosci.* **24**,
929 954–963 (2021).
- 930 26. Gharakhani, P. *et al.* Genome-wide meta-analysis identifies 127 open-angle glaucoma loci
931 with consistent effect across ancestries. *Nat. Commun.* **12**, 1258 (2021).
- 932 27. Chen, J. *et al.* The trans-ancestral genomic architecture of glycemic traits. *Nat. Genet.* **53**,
933 840–860 (2021).
- 934 28. Zhou, W. *et al.* GWAS of thyroid stimulating hormone highlights pleiotropic effects and
935 inverse association with thyroid cancer. *Nat. Commun.* **11**, 1–13 (2020).
- 936 29. Wightman, D. P. *et al.* A genome-wide association study with 1,126,563 individuals
937 identifies new risk loci for Alzheimer’s disease. *Nat. Genet.* **53**, 1276–1282 (2021).
- 938 30. Chen, M.-H. *et al.* Trans-ethnic and Ancestry-Specific Blood-Cell Genetics in 746,667
939 Individuals from 5 Global Populations. *Cell* **182**, 1198–1213.e14 (2020).
- 940 31. Wakefield, J. A Bayesian measure of the probability of false discovery in genetic
941 epidemiology studies. *Am. J. Hum. Genet.* **81**, 208–227 (2007).
- 942 32. Wakefield, J. Bayes factors for genome-wide association studies: comparison with P-
943 values. *Genet. Epidemiol.* **33**, 79–86 (2009).
- 944 33. Hormozdiari, F., Kostem, E., Kang, E. Y., Pasaniuc, B. & Eskin, E. Identifying Causal
945 Variants at Loci with Multiple Signals of Association. *Genetics* **198**, 497–508 (2014).
- 946 34. Kichaev, G. *et al.* Integrating functional data to prioritize causal variants in statistical fine-
947 mapping studies. *PLoS Genet.* **10**, e1004722 (2014).
- 948 35. Kichaev, G. & Pasaniuc, B. Leveraging Functional-Annotation Data in Trans-ethnic Fine-
949 Mapping Studies. *Am. J. Hum. Genet.* **97**, 260–271 (2015).
- 950 36. Li, D., Zhao, H. & Gelernter, J. Strong protective effect of the aldehyde dehydrogenase
951 gene (ALDH2) 504lys (*2) allele against alcoholism and alcohol-induced medical diseases
952 in Asians. *Hum. Genet.* **131**, 725–737 (2012).
- 953 37. Brown, B. C., Asian Genetic Epidemiology Network Type 2 Diabetes Consortium, Ye, C. J.,
954 Price, A. L. & Zaitlen, N. Transethnic Genetic-Correlation Estimates from Summary
955 Statistics. *Am. J. Hum. Genet.* **99**, 76–88 (2016).
- 956 38. Shi, H. *et al.* Population-specific causal disease effect sizes in functionally important
957 regions impacted by selection. *bioRxiv* 803452 (2020) doi:10.1101/803452.
- 958 39. COVID-19 Host Genetics Initiative. Mapping the human genetic architecture of COVID-19.
959 *Nature* **600**, 472–477 (2021).
- 960 40. Dendrou, C. A. *et al.* Resolving *TYK2* locus genotype-to-phenotype differences in
961 autoimmunity. *Sci. Transl. Med.* **8**, 363ra149 (2016).
- 962 41. Couturier, N. *et al.* Tyrosine kinase 2 variant influences T lymphocyte polarization and
963 multiple sclerosis susceptibility. *Brain* **134**, 693–703 (2011).
- 964 42. Li, Z. *et al.* Two rare disease-associated Tyk2 variants are catalytically impaired but
965 signaling competent. *J. Immunol.* **190**, 2335–2344 (2013).
- 966 43. Lam, M. *et al.* RICOPILI: Rapid Imputation for COnsortias PIpeLIne. *Bioinformatics* **36**,
967 930–933 (2020).
- 968 44. Huang, H. *et al.* Fine-mapping inflammatory bowel disease loci to single-variant resolution.

- 969 *Nature* **547**, 173–178 (2017).
- 970 45. Winkler, T. W. *et al.* Quality control and conduct of genome-wide association meta-
971 analyses. *Nat. Protoc.* **9**, 1192–1212 (2014).
- 972 46. Chen, W. *et al.* Improved analyses of GWAS summary statistics by reducing data
973 heterogeneity and errors. *Nat. Commun.* **12**, 7117 (2021).
- 974 47. Yang, J. *et al.* Conditional and joint multiple-SNP analysis of GWAS summary statistics
975 identifies additional variants influencing complex traits. *Nat. Genet.* **44**, 369–75, S1–3
976 (2012).
- 977 48. Buniello, A. *et al.* The NHGRI-EBI GWAS Catalog of published genome-wide association
978 studies, targeted arrays and summary statistics 2019. *Nucleic Acids Res.* **47**, D1005–
979 D1012 (2019).
- 980 49. 1000 Genomes Project Consortium *et al.* A global reference for human genetic variation.
981 *Nature* **526**, 68–74 (2015).
- 982 50. McCarthy, S. *et al.* A reference panel of 64,976 haplotypes for genotype imputation. *Nat.*
983 *Genet.* **48**, 1279–1283 (2016).
- 984 51. Taliun, D. *et al.* Sequencing of 53,831 diverse genomes from the NHLBI TOPMed Program.
985 *Nature* **590**, 290–299 (2021).
- 986 52. Schoech, A. P. *et al.* Quantification of frequency-dependent genetic architectures in 25 UK
987 Biobank traits reveals action of negative selection. *Nat. Commun.* **10**, 790 (2019).
- 988 53. Yang, J. *et al.* Genome partitioning of genetic variation for complex traits using common
989 SNPs. *Nat. Genet.* **43**, 519–525 (2011).
- 990 54. Ormond, C., Ryan, N. M., Corvin, A. & Heron, E. A. Converting single nucleotide variants
991 between genome builds: from cautionary tale to solution. *Brief. Bioinform.* **22**, (2021).
- 992 55. Asimit, J. L., Hatzikotoulas, K., McCarthy, M., Morris, A. P. & Zeggini, E. Trans-ethnic study
993 design approaches for fine-mapping. *Eur. J. Hum. Genet.* **24**, 1330–1336 (2016).
- 994 56. Marchini, J. & Howie, B. Genotype imputation for genome-wide association studies. *Nat.*
995 *Rev. Genet.* **11**, 499–511 (2010).
- 996 57. Karczewski, K. J. *et al.* The mutational constraint spectrum quantified from variation in
997 141,456 humans. *Nature* **581**, 434–443 (2020).
- 998 58. Sakaue, S. *et al.* A cross-population atlas of genetic associations for 220 human
999 phenotypes. *Nat. Genet.* **53**, 1415–1424 (2021).
- 1000 59. The GTEx Consortium. The GTEx Consortium atlas of genetic regulatory effects across
1001 human tissues. *Science* **369**, 1318–1330 (2020).
- 1002 60. Kerimov, N. *et al.* A compendium of uniformly processed human gene expression and
1003 splicing quantitative trait loci. *Nat. Genet.* **53**, 1290–1299 (2021).
- 1004 61. Koskela, J. T. *et al.* Genetic variant in SPDL1 reveals novel mechanism linking pulmonary
1005 fibrosis risk and cancer protection. *bioRxiv* (2021) doi:10.1101/2021.05.07.21255988.
- 1006 62. Partanen, J. J. *et al.* Leveraging global multi-ancestry meta-analysis in the study of
1007 Idiopathic Pulmonary Fibrosis genetics. *bioRxiv* (2021) doi:10.1101/2021.12.29.21268310.
- 1008 63. Foreman, M. G. *et al.* Alpha-1 Antitrypsin PiMZ Genotype Is Associated with Chronic
1009 Obstructive Pulmonary Disease in Two Racial Groups. *Ann. Am. Thorac. Soc.* **14**, 1280–
1010 1287 (2017).
- 1011 64. Tsuo, K. *et al.* Multi-ancestry meta-analysis of asthma identifies novel associations and
1012 highlights the value of increased power and diversity. *bioRxiv* (2021)
1013 doi:10.1101/2021.11.30.21267108.
- 1014 65. Benonisdotir, S. *et al.* Epigenetic and genetic components of height regulation. *Nat.*
1015 *Commun.* **7**, 13490 (2016).
- 1016 66. Marouli, E. *et al.* Rare and low-frequency coding variants alter human adult height. *Nature*
1017 **542**, 186–190 (2017).
- 1018 67. Langefeld, C. D. *et al.* Transancestral mapping and genetic load in systemic lupus
1019 erythematosus. *Nat. Commun.* **8**, 16021 (2017).

- 1020 68. Hargreaves, C. E. *et al.* Fcγ receptors: genetic variation, function, and disease. *Immunol.*
1021 *Rev.* **268**, 6–24 (2015).
- 1022 69. Franke, L. *et al.* Association analysis of copy numbers of FC-gamma receptor genes for
1023 rheumatoid arthritis and other immune-mediated phenotypes. *Eur. J. Hum. Genet.* **24**, 263–
1024 270 (2016).
- 1025 70. UK10K Consortium *et al.* The UK10K project identifies rare variants in health and disease.
1026 *Nature* **526**, 82–90 (2015).
- 1027 71. Wang, Y. *et al.* Global biobank analyses provide lessons for computing polygenic risk
1028 scores across diverse cohorts. *medRxiv* 2021.11.18.21266545 (2021).
- 1029 72. Namba, S. *et al.* A practical guideline of genomics-driven drug discovery in the era of global
1030 biobank meta-analysis. *bioRxiv* (2021) doi:10.1101/2021.12.03.21267280.
- 1031 73. Wu, K.-H. H. *et al.* Polygenic risk score from a multi-ancestry GWAS uncovers susceptibility
1032 of heart failure. *bioRxiv* (2021) doi:10.1101/2021.12.06.21267389.
- 1033 74. Lo Faro, V. *et al.* Genome-wide association meta-analysis identifies novel ancestry-specific
1034 primary open-angle glaucoma loci and shared biology with vascular mechanisms and cell
1035 proliferation. *bioRxiv* (2021) doi:10.1101/2021.12.16.21267891.
- 1036 75. Surakka, I. *et al.* Multi-ancestry meta-analysis identifies 2 novel loci associated with
1037 ischemic stroke and reveals heterogeneity of effects between sexes and ancestries.
1038 *bioRxiv* (2022) doi:10.1101/2022.02.28.22271647.
- 1039 76. Wolford, B. N. *et al.* Multi-ancestry GWAS for venous thromboembolism identifies novel loci
1040 followed by experimental validation in zebrafish. *medRxiv* (2022)
1041 doi:10.1101/2022.06.21.22276721.
- 1042 77. Aneas, I. *et al.* Asthma-associated genetic variants induce IL33 differential expression
1043 through an enhancer-blocking regulatory region. *Nat. Commun.* **12**, 6115 (2021).
- 1044 78. Vladich, F. D. *et al.* IL-13 R130Q, a common variant associated with allergy and asthma,
1045 enhances effector mechanisms essential for human allergic inflammation. *J. Clin. Invest.*
1046 **115**, 747–754 (2005).
- 1047 79. All of Us Research Program Investigators *et al.* The ‘All of Us’ Research Program. *N. Engl.*
1048 *J. Med.* **381**, 668–676 (2019).
- 1049 80. Farh, K. K.-H. *et al.* Genetic and epigenetic fine mapping of causal autoimmune disease
1050 variants. *Nature* **518**, 337–343 (2015).
- 1051 81. Wojcik, G. L. *et al.* Genetic analyses of diverse populations improves discovery for complex
1052 traits. *Nature* **570**, 514–518 (2019).
- 1053 82. Luo, Y. *et al.* A high-resolution HLA reference panel capturing global population diversity
1054 enables multi-ancestry fine-mapping in HIV host response. *Nat. Genet.* **53**, 1504–1516
1055 (2021).
- 1056 83. Sakaue, S. *et al.* Decoding the diversity of killer immunoglobulin-like receptors by deep
1057 sequencing and a high-resolution imputation method. *Cell Genomics* **2**, (2022).
- 1058 84. Mukamel, R. E. *et al.* Protein-coding repeat polymorphisms strongly shape diverse human
1059 phenotypes. *Science* **373**, 1499–1505 (2021).
- 1060 85. Mägi, R. *et al.* Trans-ethnic meta-regression of genome-wide association studies
1061 accounting for ancestry increases power for discovery and improves fine-mapping
1062 resolution. *Hum. Mol. Genet.* **26**, 3639–3650 (2017).
- 1063 86. Gagliano Taliun, S. A. *et al.* Exploring and visualizing large-scale genetic associations by
1064 using PheWeb. *Nat. Genet.* **52**, 550–552 (2020).
- 1065 87. Su, Z., Marchini, J. & Donnelly, P. HAPGEN2: Simulation of multiple disease SNPs.
1066 *Bioinformatics* **27**, 2304–2305 (2011).
- 1067 88. Manichaikul, A. *et al.* Robust relationship inference in genome-wide association studies.
1068 *Bioinformatics* **26**, 2867–2873 (2010).
- 1069 89. Chang, C. C. *et al.* Second-generation PLINK: rising to the challenge of larger and richer
1070 datasets. *Gigascience* **4**, 7 (2015).

- 1071 90. Wei, X. & Nielsen, R. CCR5- Δ 32 is deleterious in the homozygous state in humans. *Nat.*
1072 *Med.* **25**, 909–910 (2019).
1073 91. Maier, R. *et al.* No statistical evidence for an effect of CCR5- Δ 32 on lifespan in the UK
1074 Biobank cohort. *Nat. Med.* **26**, 178–180 (2020).
1075 92. Das, S. *et al.* Next-generation genotype imputation service and methods. *Nat. Genet.* **48**,
1076 1284–1287 (2016).
1077 93. Loh, P.-R. *et al.* Reference-based phasing using the Haplotype Reference Consortium
1078 panel. *Nat. Genet.* **48**, 1443–1448 (2016).
1079 94. Loh, P.-R. *et al.* Contrasting genetic architectures of schizophrenia and other complex
1080 diseases using fast variance-components analysis. *Nat. Genet.* **47**, 1385–1392 (2015).
1081 95. McLaren, W. *et al.* The Ensembl Variant Effect Predictor. *Genome Biol.* **17**, 122 (2016).

1082

1083 Global Biobank Meta-analysis Initiative

1084 Wei Zhou^{1,2,3}, Masahiro Kanai^{1,2,3,4,5}, Kuan-Han H Wu⁶, Humaira Rasheed^{7,8,9}, Kristin Tsuo^{1,2,3},
1085 Jibril B Hirbo^{10,11}, Ying Wang^{1,2,3}, Arjun Bhattacharya¹², Huiling Zhao⁹, Shinichi Namba⁵, Ida
1086 Surakka¹³, Brooke N Wolford^{6,7}, Valeria Lo Faro^{14,15,16}, Esteban A Lopera-Maya¹⁷, Kristi Läll¹⁸,
1087 Marie-Julie Favé¹⁹, Juulia J Partanen²⁰, Sinéad B Chapman^{2,3}, Juha Karjalainen^{1,2,3,20}, Mitja
1088 Kurki^{1,2,3,20}, Mutaamba Maasha^{1,2,3,20}, Ben M Brumpton^{7,21,22}, Sameer Chavan²³, Tzu-Ting Chen²⁴,
1089 Michelle Daya²³, Yi Ding^{25,12}, Yen-Chen A Feng²⁶, Lindsay A Guare²⁷, Christopher R Gignoux²³,
1090 Sarah E Graham¹³, Whitney E Hornsby¹³, Nathan Ingold^{28,29}, Said I. Ismail³⁰, Ruth Johnson^{31,12},
1091 Triin Laisk¹⁸, Kuang Lin³², Jun Lv³³, Iona Y Millwood^{32,34}, Sonia Moreno-Grau³⁵, Kisung Nam³⁶,
1092 Priit Palta^{18,20}, Anita Pandit³⁷, Michael H Preuss³⁸, Chadi Saad³⁰, Shefali S Setia³⁹, Unnur
1093 Thorsteinsdottir⁴⁰, Jasmina Uzunovic¹⁹, Anurag Verma^{41,42}, Matthew Zawistowski³⁷, Xue
1094 Zhong^{10,11}, Nahla Afifi⁴³, Kawthar M. Al-Dabhani⁴³, Asma Al Thani⁴³, Yuki Bradford²⁷, Archie
1095 Campbell⁴⁴, Kristy Crooks²³, Geertruida H de Bock⁴⁵, Scott M Damrauer^{46,27,42}, Nicholas J
1096 Douville^{47,48}, Sarah Finer⁴⁹, Lars G Fritsche³⁷, Eleni Fthenou⁴³, Gilberto Gonzalez-Arroyo^{35,50},
1097 Christopher J Griffiths⁴⁹, Yu Guo⁵¹, Karen A Hunt⁵², Alexander Ioannidis^{35,53}, Nomdo M
1098 Jansonius¹⁴, Takahiro Konuma^{5,54}, Ming Ta Michael Lee³⁵, Arturo Lopez-Pineda^{35,50}, Yuta
1099 Matsuda⁵⁵, Riccardo E Marioni⁴⁴, Babak Moatamed³⁵, Marco A Nava-Aguilar^{35,50}, Kensuke
1100 Numakura⁵⁵, Snehal Patil³⁷, Nicholas Rafaels²³, Anne Richmond⁵⁶, Agustin Rojas-Muñoz³⁵,
1101 Jonathan A Shortt²³, Peter Straub^{10,11}, Ran Tao^{57,11}, Brett Vanderwerff³⁷, Manvi Vernekar⁵⁵,
1102 Yogasudha Veturi²⁷, Kathleen C Barnes²³, Marike Boezen^{45,†}, Zhengming Chen^{32,34}, Chia-Yen
1103 Chen⁵⁸, Judy Cho³⁸, George Davey Smith^{9,59}, Hilary K Finucane^{1,3,2}, Lude Franke¹⁷, Eric R
1104 Gamazon^{10,11,60}, Andrea Ganna^{1,2,20}, Tom R Gaunt^{9,59}, Tian Ge^{61,62}, Hailiang Huang^{1,2}, Jennifer
1105 Huffman⁶³, Nicholas Katsanis³⁵, Jukka T Koskela²⁰, Clara Lajonchere^{64,65}, Matthew H Law^{28,29},
1106 Liming Li³³, Cecilia M Lindgren⁶⁶, Ruth JF Loos^{38,67}, Stuart MacGregor²⁸, Koichi Matsuda⁶⁸,
1107 Catherine M Olsen²⁸, David J Porteous⁴⁴, Jordan A Shavit⁶⁹, Harold Snieder⁴⁵, Tomohiro
1108 Takano⁵⁵, Richard C Trembath⁷⁰, Judith M Vonk⁴⁵, David C. Whiteman²⁸, Stephen J Wicks²³,
1109 Cisca Wijmenga¹⁷, John Wright⁷¹, Jie Zheng⁹, Xiang Zhou³⁷, Philip Awadalla^{19,72}, Michael
1110 Boehnke³⁷, Carlos D Bustamante^{35,53,73}, Nancy J Cox^{10,11}, Segun Fatumo^{74,75,76}, Daniel H
1111 Geschwind^{77,64,78}, Caroline Hayward⁵⁶, Kristian Hveem^{7,21}, Eimear E Kenny⁷⁹, Seunggeun Lee³⁶,
1112 Yen-Feng Lin^{24,80,81}, Hamdi Mbarek³⁰, Reedik Mägi¹⁸, Hilary C Martin⁸², Sarah E Medland²⁸,
1113 Yukinori Okada^{5,83,84,85,86}, Aarno V Palotie^{1,2,20}, Bogdan Pasaniuc^{12,77,87,25,64}, Daniel J Rader^{27,41},
1114 Marylyn D Ritchie²⁷, Serena Sanna^{88,17}, Jordan W Smoller⁶¹, Kari Stefansson⁴⁰, David A van
1115 Heel⁵², Robin G Walters^{32,34}, Sebastian Zöllner³⁷, Biobank of the Americas, Biobank Japan
1116 Project, BioMe, BioVU, CanPath - Ontario Health Study, China Kadoorie Biobank Collaborative
1117 Group, Colorado Center for Personalized Medicine, deCODE Genetics, Estonian Biobank,
1118 FinnGen, Generation Scotland, Genes & Health Research Team, LifeLines, Mass General
1119 Brigham Biobank, Michigan Genomics Initiative, National Biobank of Korea, Penn Medicine
1120 BioBank, Qatar Biobank, The QSkin Sun and Health Study, Taiwan Biobank, The HUNT Study,
1121 UCLA ATLAS Community Health Initiative, Uganda Genome Resource, UK Biobank, Alicia R
1122 Martin^{1,2,3}, Cristen J Willer^{13,6,89*}, Mark J Daly^{1,2,3,20*}, Benjamin M Neale^{1,2,3*}

1123

1124 †Deceased

1125 *These authors jointly supervised the initiative

1126

1127 ¹Analytic and Translational Genetics Unit, Department of Medicine, Massachusetts General
1128 Hospital, Boston, MA, USA, ²Stanley Center for Psychiatric Research, Broad Institute of MIT and
1129 Harvard, Cambridge, MA, USA, ³Program in Medical and Population Genetics, Broad Institute of

1130 MIT and Harvard, Cambridge, MA, USA, ⁴Department of Biomedical Informatics, Harvard Medical
1131 School, Boston, MA, USA, ⁵Department of Statistical Genetics, Osaka University Graduate
1132 School of Medicine, Suita 565-0871, Japan, ⁶Department of Computational Medicine and
1133 Bioinformatics, University of Michigan, Ann Arbor, MI, USA, ⁷K.G. Jebsen Center for Genetic
1134 Epidemiology, Department of Public Health and Nursing, NTNU, Norwegian University of Science
1135 and Technology, Trondheim, Norway, ⁸Division of Medicine and Laboratory Sciences, University
1136 of Oslo, Norway, ⁹MRC Integrative Epidemiology Unit (IEU), Bristol Medical School, University of
1137 Bristol, Bristol, UK, ¹⁰Department of Medicine, Division of Genetic Medicine, Vanderbilt University
1138 Medical Center, Nashville, TN, USA, ¹¹Vanderbilt Genetics Institute, Vanderbilt University Medical
1139 Center, Nashville, TN, USA, ¹²Department of Pathology and Laboratory Medicine, David Geffen
1140 School of Medicine, University of California, Los Angeles, Los Angeles, CA, USA, ¹³Department
1141 of Internal Medicine, Division of Cardiology, University of Michigan, Ann Arbor, MI, USA,
1142 ¹⁴University of Groningen, UMCG, Department of Ophthalmology, Groningen, the Netherlands,
1143 ¹⁵Department of Clinical Genetics, Amsterdam University Medical Center (AMC), Amsterdam, the
1144 Netherlands, ¹⁶Department of Immunology, Genetics and Pathology, Science for Life Laboratory,
1145 Uppsala University, Uppsala, Sweden, ¹⁷University of Groningen, UMCG, Department of
1146 Genetics, Groningen, the Netherlands, ¹⁸Estonian Genome Centre, Institute of Genomics,
1147 University of Tartu, Tartu, Estonia, ¹⁹Ontario Institute for Cancer Research, Toronto, ON, Canada,
1148 ²⁰Institute for Molecular Medicine Finland, University of Helsinki, Helsinki, Finland, ²¹HUNT
1149 Research Centre, Department of Public Health and Nursing, NTNU, Norwegian University of
1150 Science and Technology, Levanger, Norway, ²²Clinic of Medicine, St. Olavs Hospital, Trondheim
1151 University Hospital, Trondheim, Norway, ²³University of Colorado - Anschutz Medical Campus,
1152 Aurora, CO, USA, ²⁴Center for Neuropsychiatric Research, National Health Research Institutes,
1153 Miaoli, Taiwan, ²⁵Bioinformatics Interdepartmental Program, University of California, Los Angeles,
1154 Los Angeles, CA, USA, ²⁶Division of Biostatistics, Institute of Epidemiology and Preventive
1155 Medicine, College of Public Health, National Taiwan University, Taiwan, ²⁷Department of
1156 Genetics, Perelman School of Medicine, University of Pennsylvania, Philadelphia, PA, USA,
1157 ²⁸QIMR Berghofer Medical Research Institute, Brisbane, Australia, ²⁹Faculty of Health, School of
1158 Biomedical Sciences, Queensland University of Technology, Australia, ³⁰Qatar Genome Program,
1159 Qatar Foundation Research, Development and Innovation, Qatar Foundation, Doha, Qatar,
1160 ³¹Department of Computer Science, University of California, Los Angeles, Los Angeles, CA, USA,
1161 ³²Nuffield Department of Population Health, University of Oxford, Oxford, UK, ³³Department of
1162 Epidemiology and Biostatistics, School of Public Health, Peking University Health Science Center,
1163 Beijing, China, ³⁴MRC Population Health Research Unit, University of Oxford, Oxford, UK,
1164 ³⁵Galatea Bio Inc., Hialeah, FL, USA, ³⁶Graduate School of Data Science, Seoul National
1165 University, ³⁷Department of Biostatistics and Center for Statistical Genetics, University of
1166 Michigan, Ann Arbor, MI, USA, ³⁸The Charles Bronfman Institute for Personalized Medicine, Icahn
1167 School of Medicine at Mount Sinai, New York, NY, USA, ³⁹Department of Pathology and
1168 Laboratory Medicine, Perelman School of Medicine, University of Pennsylvania, Philadelphia, PA,
1169 USA, ⁴⁰deCODE Genetics/Amgen inc., 101, Reykjavik, Iceland, ⁴¹Department of Medicine,
1170 Perelman School of Medicine, University of Pennsylvania, Philadelphia, PA, USA, ⁴²Corporal
1171 Michael Crescenzo VA Medical Center, Philadelphia, PA, USA, ⁴³Qatar Biobank for Medical
1172 Research, Qatar Foundation for Education, Science, and Community, Doha, Qatar, ⁴⁴Centre for
1173 Genomic and Experimental Medicine, Institute of Genetics and Cancer, University of Edinburgh,
1174 Edinburgh, UK, ⁴⁵Department of Epidemiology, University Medical Center Groningen, Groningen,
1175 the Netherlands, ⁴⁶Department of Surgery, Perelman School of Medicine, University of
1176 Pennsylvania, Philadelphia, PA, USA, ⁴⁷Department of Anesthesiology, Michigan Medicine, Ann
1177 Arbor, MI, USA, ⁴⁸Institute of Healthcare Policy & Innovation, University of Michigan, Ann Arbor,
1178 MI, USA, ⁴⁹Wolfson Institute of Population Health, Queen Mary University of London, London,
1179 UK, ⁵⁰Amphora Health, Morelia, Michoacan, Mexico, ⁵¹Chinese Academy of Medical Sciences,
1180 Beijing, China, ⁵²Blizard Institute, Queen Mary University of London, London, UK, ⁵³Stanford

1181 University School of Medicine, Stanford, CA, USA, ⁵⁴Central Pharmaceutical Research Institute,
1182 JAPAN TOBACCO INC., Takatsuki 569-1125, Japan, ⁵⁵Genomelink, Inc., Berkeley, CA, USA,
1183 ⁵⁶Medical Research Council Human Genetics Unit, Institute of Genetics and Cancer, University
1184 of Edinburgh, Edinburgh, UK, ⁵⁷Department of Biostatistics, Vanderbilt University Medical Center,
1185 Nashville, TN, USA, ⁵⁸Biogen, Cambridge, MA, USA, ⁵⁹NIHR Bristol Biomedical Research Centre,
1186 Bristol, UK, ⁶⁰MRC Epidemiology Unit, University of Cambridge, Cambridge, UK, ⁶¹Psychiatric
1187 and Neurodevelopmental Genetics Unit, Center for Genomic Medicine, Massachusetts General
1188 Hospital, Boston, MA, USA, ⁶²Center for Precision Psychiatry, Massachusetts General Hospital,
1189 Boston, MA, USA, ⁶³Centre for Population Genomics, VA Boston Healthcare System, Boston,
1190 MA, USA, ⁶⁴Institute of Precision Health, University of California, Los Angeles, Los Angeles, CA,
1191 USA, ⁶⁵Program in Neurogenetics, Department of Neurology, David Geffen School of Medicine,
1192 University of California, Los Angeles, Los Angeles, CA, USA, ⁶⁶Big Data Institute, Li Ka Shing
1193 Centre for Health Information and Discovery, University of Oxford, Oxford, UK, ⁶⁷Novo Nordisk
1194 Foundation Center for Basic Metabolic Research, Faculty of Medicine and Health Sciences,
1195 University of Copenhagen, Copenhagen, Denmark, ⁶⁸Department of Computational Biology and
1196 Medical Sciences, Graduate school of Frontier Sciences, The University of Tokyo, Tokyo, Japan,
1197 ⁶⁹University of Michigan, Department of Pediatrics, Ann Arbor MI 48109, ⁷⁰School of Basic and
1198 Medical Biosciences, Faculty of Life Sciences and Medicine, King's College London, London, UK,
1199 ⁷¹Bradford Institute for Health Research, Bradford Teaching Hospitals National Health Service
1200 (NHS) Foundation Trust, Bradford, UK, ⁷²Department of Molecular Genetics, University of
1201 Toronto, Toronto, ON, Canada, ⁷³Chan Zuckerberg Biohub, San Francisco, CA, USA, ⁷⁴The
1202 African Computational Genomics (TACG) Research Group, MRC/UVRI and LSHTM, Entebbe,
1203 Uganda, ⁷⁵London School of Hygiene & Tropical Medicine London, UK, ⁷⁶Medical Research
1204 Council/ Uganda Virus Research Institute/London School of Hygiene and Tropical Medicine
1205 (MRC/UVRI/LSHTM) Uganda research unit, Entebbe, Uganda, ⁷⁷Department of Human Genetics,
1206 David Geffen School of Medicine, University of California, Los Angeles, Los Angeles, CA, USA,
1207 ⁷⁸Department of Neurology, David Geffen School of Medicine, University of California, Los
1208 Angeles, Los Angeles, CA, USA, ⁷⁹Institute for Genomic Health, Icahn School of Medicine at
1209 Mount Sinai, New York, NY, USA, ⁸⁰Department of Public Health & Medical Humanities, School
1210 of Medicine, National Yang Ming Chiao Tung University, Taipei, Taiwan, ⁸¹Institute of Behavioral
1211 Medicine, College of Medicine, National Cheng Kung University, Tainan, Taiwan, ⁸²Medical and
1212 Population Genomics, Wellcome Sanger Institute, Hinxton, UK, ⁸³Department of Genome
1213 Informatics, Graduate School of Medicine, the University of Tokyo, Tokyo 113-0033, Japan.,
1214 ⁸⁴Laboratory of Statistical Immunology, Immunology Frontier Research Center (WPI-IFReC),
1215 Osaka University, Suita 565-0871, Japan, ⁸⁵Laboratory for Systems Genetics, RIKEN Center for
1216 Integrative Medical Sciences, Yokohama, Japan, ⁸⁶Integrated Frontier Research for Medical
1217 Science Division, Institute for Open and Transdisciplinary Research Initiatives, Osaka University,
1218 Suita 565-0871, Japan, ⁸⁷Department of Computational Medicine, David Geffen School of
1219 Medicine, University of California, Los Angeles, Los Angeles, CA, USA, ⁸⁸Institute for Genetics
1220 and Biomedical Research (IRGB), National Research Council (CNR), Cagliari, Italy, ⁸⁹Department
1221 of Human Genetics, University of Michigan, Ann Arbor, MI, USA

1222

1223

1224